Nelson KG, Takahashi T, Lee DC, Luetteke NC, Bossert NL, Ross K, Eitzman BE and McLachlan JA. (1992). *Endocrinology*, **131**, 1657–1664.

Normanno N, Selvam MP, Qi CF, Saeki T, Johnson G, Kim N, Ciardiello F, Shoyab M, Plowman G, Brandt R, Todaro G and Salomon DS. (1994). *Proc. Natl. Acad. Sci. USA*, **91**, 2790–2794.

Pastan I and Willingham MC. (1983). *Trends Biochem. Sci.*, **8**, 250–254.

Piepkorn M, Lo C and Plowman G. (1994). *J. Cell. Physiol.*, **159**, 114–120.

Sato T, Fukazawa Y, Kojima H, Ohta Y and Iguchi T. (2003). *Reprod. Toxicol.*, **17**, 289–297.

Sato T, Fukazawa Y, Kojima H, Ohta Y, Tomooka Y and Iguchi T. (1996a). *Proceedings of the 10th International Congress on Endocrinology, San Francisco*, San Francisco, pp. 1–254.

Sato T, Ohta Y, Okamura H, Hayashi S and Iguchi T. (1996b). *Anat. Rec.*, **244**, 374–385.

Takasugi N. (1976). *Int. Rev. Cytol.*, **44**, 193–224.

Takasugi N, Bern HA and DeOme KB. (1962). *Science*, **138**, 438–439.

Tsai PS, Uchima F-DA, Hamamoto ST and Bern HA. (1991). *In vitro Cell Dev. Biol.*, **27A**, 461–468.

Yee D and Lee AV. (2000). *J. Mammary Gland Biol. Neoplasia*, **5**, 107–115.

The estrogen-responsive adrenomedullin and receptor-modifying protein 3 gene identified by DNA microarray analysis are directly regulated by estrogen receptor

H Watanabe, E Takahashi, M Kobayashi, M Goto, A Krust[1], P Chambon[1] and T Iguchi

Okazaki Institute for Integrative Bioscience, National Institutes of Natural Science, 5-1 Higashiyama, Myodaiji, Okazaki 444-8787, Japan and Core Research for Evolution Science and Technology (CREST), Japan Science and Technology Corporation

[1]Institut de Génétique et de Biologie Moléculaire et Cellulaire, Centre National de la Recherche Scientifique, Institut National de la Santé et de la Recherche Médicale, Université Louis Pasteur, Collége de France, 67404 Illkirch, Strasbourg, France

(Requests for offprints should be addressed to T Iguchi; Email: taisen@nibb.ac.jp)

Abstract

Recent studies have revealed that hundreds of genes in the uterus are activated by estrogen. Their expression profiles differ over time and doses and it is not clear whether all these genes are directly regulated by estrogen via the estrogen receptor. To select the genes that may be regulated by estrogen, we treated mice with several doses of estrogen and searched for those genes whose dose–response expression pattern mirrored the uterine growth pattern. Among those genes, we found that the dose-dependent expression of the adrenomedullin (ADM) gene correlated well with the uterotrophic effect of estrogen. ADM expression is induced early after estrogen administration and is restricted to the endometrial stroma. The spatiotemporal gene expression pattern of ADM was similar to that of receptor-modifying protein 3 (RAMP3). RAMP3 is known to modify calcitonin gene-related receptor (CRLR) so that it can then serve as an ADM receptor. Chromatin immunoprecipitation assays indicated that the estrogen receptor binds directly to the ADM promoter region and RAMP3 intron after estrogen administration. It was also shown that neither the ADM nor RAMP3 gene could be activated in estrogen receptor-α-null mouse. Although uterine ADM expression has been reported to occur in the myometrium, our observations indicate that estrogen-induced ADM is also expressed in the uterine stroma and that such variable, spatiotemporally regulated ADM expression contributes to a wider range of biological effects than previously expected.

Journal of Molecular Endocrinology (2006) **36,** 81–89

Introduction

The uterus is a major target organ of estrogen and undergoes drastic changes after estrogen administration. Early uterine responses to estrogen include many physiological biochemical changes such as hyperemia, calcium influx, histamine release, eosinophil infiltration, cAMP level changes, enhanced glucose oxidation, and increased RNA and protein synthesis. After DNA synthesis and mitosis, later stage effects include cellular hypertrophy and hyperplasia and the result is the growth of the uterus. This uterotrophic effect of estrogen is a demonstrable phenotype that can be used to estimate the potency of estrogens. Notably, not all the physiological and biochemical changes associated with estrogen treatment are necessary for the uterotrophic effect. For example, while cAMP is elevated after estrogen administration (Szego & Davis 1967), uterine growth is independent of cAMP (Zor *et al.* 1973). This is also true for ornithine decarboxylation and prostaglandins. Thus, it remains unclear which processes are essential for the effects of estrogen in target tissues.

In the level of gene expression, it is also not clear whether estrogen-response genes are directly regulated by estrogen receptor (ER) or not. Recently, the effect of estrogen on the uterus has been studied at the level of gene expression by DNA microarray analysis (Watanabe *et al.* 2002). As a result, hundreds of genes have been listed as being estrogen-responsive and the temporal changes in their expression after estrogen exposure have been analyzed (Watanabe *et al.* 2003). This has vastly aided our understanding of the effect of estrogen on the uterus at the genetic level. However, this new methodology, like the classical methodology, cannot determine whether a particular gene-expression change is the direct effect of estrogen or not.

In our previous study we found that not all estrogen-responsive genes are uniformly activated by estrogen and that their estrogen-dose-dependent, gene-expression patterns are not necessarily identical with the uterotrophic effect of estrogen (Watanabe *et al.* 2003). For example, while the uterotrophic effect of estrogen is directly proportional to the estrogen doses used, some

Journal of Molecular Endocrinology (2006) **36,** 81–89
0952–5041/06/036–081 *Printed in Great Britain*

DOI: 10.1677/jme.1.01825
Online version via http://www.endocrinology-journals.org

genes are activated by a low dose of estrogen but this activation is saturated or diminished by higher doses of estrogen. These various estrogen-response patterns are generally attributed to the differences of promoter context but the contribution of ER is not clear. In this study, we selected the adrenomedullin (ADM) and receptor-modifying protein 3 (RAMP3) genes, whose expression patterns correlate closely with the uterotrophic effect, and studied the direct contribution of ER to their expression.

Experimental procedures

Animals

Female C57BL/6J mice and ERα- and -β-null mice (Dupont *et al.* 2000) were housed under a 12 h:12 h light/darkness cycle. To assess the effect of estrogen on uterine gene expression, mice were ovariectomized at 8 weeks of age and 2 weeks later injected intraperitoneally with estrogen (or sesame oil as a vehicle control; Nakarai Tesque, Kyoto, Japan). The whole uterus ($n=4$) were collected 6 h later. The estrogen used was 17β-estradiol (Sigma-Aldrich Japan, Tokyo, Japan) and it was injected at 0·05, 0·5, 5 or 50 μg/kg body weight (b.w.). To assess the effects of the different estrogen doses on uterine growth, mice were ovariectomized and 2 weeks later injected intraperitoneally every 24 h for 7 days with the different 17β-estradiol doses or sesame oil. The whole uterus ($n=5$) were then collected and weighed. All animal experiments were approved by the institutional animal care committee.

Preparation of labeled cRNA and microarray analysis

Total uterine RNA was extracted using TRIzol reagent (Invitrogen, Tokyo, Japan) and cRNA probes were prepared from the purified RNA by using an Affymetrix cRNA probe kit according to the manufacturer's protocol (Affymetrix Japan, Tokyo, Japan). All preparations met the recommended criteria of Affymetrix for use on their expression arrays. The amplified cRNA was hybridized to high-density oligonucleotide arrays (Mouse U74 A; Affymetrix Japan), and the scanned data were analyzed with GeneChip software (Affymetrix Japan) and processed as described previously (Watanabe *et al.* 2002). To confirm the estrogen-related changes in gene expression revealed by the DNA microarray analysis, we independently repeated the same experiment at least twice. The expression data were analyzed with GeneSpring software (Agilent Tech. Japan, Tokyo, Japan).

Quantitative real-time PCR

cDNA was synthesized from total RNA purified as described above by using Superscript II reverse transcriptase (Invitrogen) with random primers at 42 °C for 60 min. Quantitative PCRs were performed by using the PE Prism 7000 sequence detector (Applied Biosystems, Tokyo, Japan), SYBR-Green PCR core reagents (Applied Biosystems) and the appropriate primers according to the manufacturer's instructions. The primers were chosen to amplify short PCR products (<100 bp), and their sequences were as follows: RAMP1 (NM_016894), 5′-TTTCATTGCGCTCCCCATT-3′ and 5′-CCAGACCACCAGTGCAGTCAT-3′; RAMP2 (NM_019444), 5′-AGTTGCATGGACTCTGTCAAG GA-3′ and 5′-TGCCTGCTAATCAAAGTCCAGTT-3′; RAMP3 (NM_019511), 5′-CCGGATGAAGTACT CATCCCA-3′ and 5′-CCACCAGGCCAGCCATAG-3′; ADM (U77630) 5′-ATAAGCCTCATTACTACTT GAACT-3′ and 5′-TTGCACGTTCCTCGCTAGGT-3′, and CRLR (calcitonin gene-related receptor; NM_018782) 5′-CACTCTGATGCTCTCCGCAGT-3′ and 5′-GGCTGTACCCTTGCATGTCAC-3′. Gene-expression levels were normalized to the expression levels of NM_012053 (ribosome L8, Rpl8), whose primer sequences were 5′-ACAGAGCCGTTGTTGGTGT TG-3′ and 5′-CAGCAGTTCCTCTTTGCCTTGT-3′. Gel electrophoresis and melting-curve analyses were performed to confirm correct amplicon size and the absence of nonspecific bands.

In situ hybridization

In situ hybridization was performed using PCR fragments containing a portion of the ADM gene (nucleotides 58–586; U77630), the RAMP2 gene (nucleotides 160–706; NM_019444) or the RAMP3 gene (nucleotides 681–1059; NM_019511). [α-^{35}S]UTP (Amersham Biosciences, Tokyo, Japan)-labeled antisense and sense RNAs were obtained by using T7 and T3 RNA polymerases and an *in vitro* transcription kit (Stratagene, Funakoshi, Tokyo, Japan). After DNase digestion, the probes were fragmented by alkali hydrolysis. The tissues were embedded in compound (Sakura Fintechnical Co., Ltd., Tokyo, Japan) and sectioned (10 μm) using a cryostat. Sections were fixed on slides with 4% paraformaldehyde for 10 min and rinsed in PBS. The slides were then acetylated in 0·1 M triethanolamine with a 1/400 vol. acetic anhydride, rinsed again in PBS, and dehydrated in graded ethanol. After air drying, the hybridization mixture was added. Hybridization was performed at 50 °C overnight with 5×10^7 d.p.m./ml probe in 100 μl hybridization solution under coverslips. After the hybridization, the slides were washed and incubated in RNase A solution (20 μg/ml) at 37 °C for 30 min, and then dipped in NTB-2 nuclear track emulsion (Kodak, Rochester, NY, USA). After 14 days exposure, the slides were developed and counterstained with hematoxylin. The sections were evaluated and photographed under dark-field illumination using a Zeiss microscope. The dark-field (changed to red) and bright-field images were merged.

Chromatin immunoprecipitation

Mouse uteri were fixed with 1% formaldehyde and homogenized using physcotron (NS-310E; Microtec, Chiba, Japan) in PBS containing 0·125 M glycine. The samples were then centrifuged at 700 ***g*** for 5 min at 4 °C and the pellets were incubated with lysis buffer (10 mM Tris/HCl, pH 8·0, 10 mM EDTA, 0·5 mM EGTA and 0·25% Triton X-100) for 10 min. The samples were collected by microcentrifugation, suspended in sonication buffer (10 mM Tris/HCl, pH 8·0, 100 mM NaCl, 1 mM EDTA and 0·5 mM EGTA), and sonicated with a Bioruptor sonicator (Cosmo Bio, Tokyo, Japan) to an average length of approximately 500 bp. The samples were precleared by treatment with Protein G–Sepharose for 1 h at 4 °C and then incubated with 10 μg anti-ERα polyclonal rabbit antibody (Santa Cruz Biotechnology, Santa Cruz, CA, USA) or anti-acetylated histone H3 antibody (Cell Signaling, Beverly, MA, USA) overnight at 4 °C. After precipitation by the addition of Protein G–Sepharose the samples were washed five times with RIPA buffer (10 mM Tris/HCl, pH 8·0, 140 mM NaCl, 1 mM EDTA, 0·5 mM EGTA, 1% Triton X-100, 0·1% SDS and 0·1% sodium deoxycholate). The precipitated samples were recovered by incubation with elution buffer (0·1 M sodium bicarbonate and 1% SDS). Crosslinks were reversed by incubation at 65 °C for 6 h followed by incubation with proteinase K at 45 °C for 4 h. Thereafter, the samples were extracted with phenol/chloroform and the DNA fragments were precipitated with a 1/10 vol. of NaCl and 2·5 vol. of ethanol. Generally, 1/30 of the precipitated DNA was used for PCR amplification. PCR amplification was performed in the presence of 0·1 nmol primers, 0·2 mM each nucleotide (dATP, dCTP, dGTP and dTTP), 1 × PCR buffer and 1 U AmpliTaq Gold (PerkinElmer Japan, Tokyo, Japan) in 20 μl of reaction buffer. After 35 cycles of amplification the amplified DNA was analyzed by agarose electrophoresis. As a negative control the same experiments were performed with IgG: no amplified DNA was obtained. The primer sequences used to amplify the putative estrogen-response element (ERE) of the ADM gene were (−796) 5′-ATCCTCA CGTTTATGATGGA-3′ (−777) and (−565) 5′-CGG ATTTCGTAATAAGGGCA-3′ (−584). The primer sequences used to amplify the putative ERE of the RAMP3 gene were (13 531 bp from the 5′ end of the first intron) 5′-AGAGTGTACGTGTGGACAGG-3′ (13 550 bp) and (13 735 bp from the 5′ end of the first intron) 5′-CTGTGACAGCAGGAGGACAG-3′ (13 716).

Results

The ADM gene expression pattern correlates well with the uterotrophic effect of estrogen

To select genes that may be involved in the estrogen-induced uterine response, we injected ovariectomized mice with four different doses of estradiol and harvested the uteri 6 h later. The total uterine RNAs were then subjected to DNA microarray analysis, which determined the expression levels of 10 000 genes. The average gene-expression levels were compared with the estrogen dose response of uterine growth (determined by daily injecting ovariectomized mice for a week with the four different estrogen doses and then weighing the whole uteri; Fig. 1A). The genes whose expression levels correlated well with the uterotrophic effect of estrogen were selected.

Of the 10 000 genes examined, 338 had a correlation coefficient of greater than 0·95. The average expression levels of these genes, as determined by the microarray analysis, are shown in Fig. 1B. The 338 selected genes included the ADM gene (Fig. 1C). In addition, the RAMP3 gene displays a similar estrogen-induced expression pattern, as shown by Fig. 1D. This is of interest because RAMP3 modifies the calcitonin gene-related receptor (CRLR), after which CRLR can serve as a receptor for ADM (McLatchie *et al.* 1998). However, CRLR gene expression was unaffected by estrogen treatment (Fig. 1D). The good correlation between ADM and RAMP3 gene expression prompted us to examine the gene-expression regulation of ADM and RAMP3 by estrogen.

ADM and RAMP3 gene expression are activated early after estrogen administration

To examine the temporal changes in ADM gene expression by estrogen exposure, we injected ovariectomized mice with 5 μg/kg b.w. estradiol, harvested the uteri 1, 2, 4 or 6 h later, and subjected the whole uterine RNA to quantitative PCR to evaluate ADM expression. The experiment was performed three times. While ADM gene expression in the uteri varied quite widely 2–4 h after estrogen administration, it was elevated 1 h after estrogen administration and continued to increase thereafter until around 4 h after estrogen administration, after which ADM expression started to decrease (Fig. 2A). Thus ADM gene expression was induced early after estrogen stimulation. RAMP3 gene expression was also induced immediately after estrogen administration and continued until 4 h after estrogen administration (Fig. 2B).

There is also another modifying protein that confers ADM receptor function onto CRLR, namely RAMP2 (McLatchie *et al.* 1998). However, we found RAMP2 expression was not effectively activated by estrogen (Fig. 2C). Moreover, RAMP1, a third CRLR-modifying protein that modifies CRLR to act as a receptor for calcitonin-gene-related peptide (CGRP; McLatchie *et al.* 1998), was substantially repressed by estrogen (Fig. 2C). Furthermore, CGRP, which binds to receptors bearing RAMP3 or RAMP1 (McLatchie *et al.* 1998), was

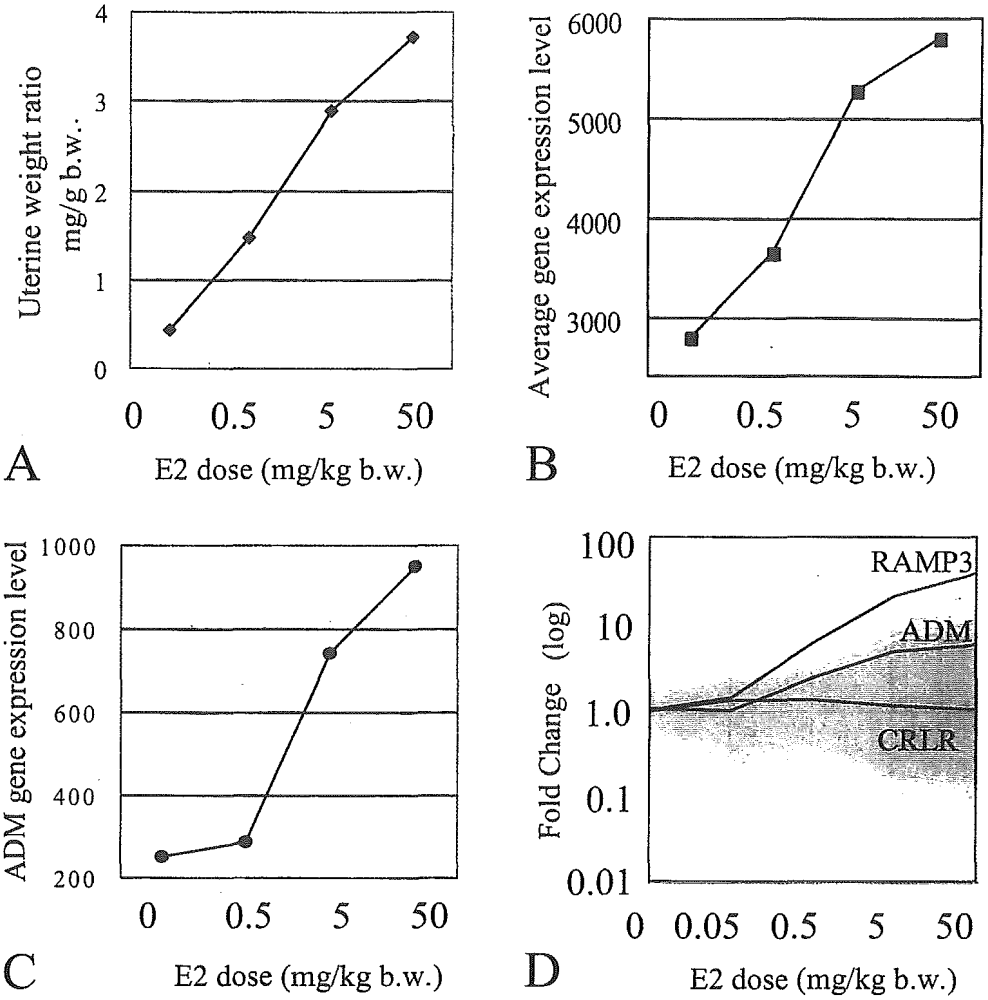

Figure 1 Correlation between estrogen dose-dependent uterine ADM gene expression and the uterotrophic effect of estrogen. (A) Uterotrophic effect of estrogen. Estrogen dose-dependent uterine growth is indicated by a ratio to body weight. (B) Average gene-expression levels of the selected genes; 338 genes whose expression correlated well with the uterotrophic effect were selected and the average gene-expression levels of the 338 genes at the different estrogen doses (calculated from the fluorescent signal intensity of each gene in the DNA microarray analysis) are indicated. (C) Estrogen-dependent gene activation of ADM gene. The gene-expression level of ADM (one of the 338 genes) is indicated. The *x* axis indicates the estradiol dose administered while the *y* axis indicated the gene-expression levels. (D) Estrogen dose-dependent changes in ADM, RAMP3 and CRLR gene expression (solid lines) relative to their expression levels at 0 μg/kg b.w. estradiol (fold expression). Gene expression of all the 10 000 genes examined is shown in gray. While ADM and RAMP3 gene expression were activated by estrogen, CRLR gene expression was not changed. The *x* axis indicates the estradiol dose administered while the *y* axis indicates fold changes in gene expression on a log scale. Note that because of the normalization algorithm, the gray gene expression is not exactly 1·0 but spread around 1·0 at the 0 mg/kg b.w. dose. E2, 17β-estradiol.

expressed in the absence of estrogen at much lower levels than ADM and was unaltered by estrogen administration (data not shown).

To examine how the expression levels of RAMP3 relate to CRLR expression upon estrogen exposure, the ratio of RAMP3 mRNA to CRLR mRNA was calculated from data obtained by quantitative PCR. As indicated in Fig. 1D, CRLR expression is unaltered by estrogen. Although RAMP3 mRNA levels were one-tenth of those of CRLR before estrogen administration, estrogen induced RAMP3 gene transcription, with the result that RAMP3 and CRLR were expressed at equivalent levels 2 h after estrogen administration, shown by mRNA levels. Although protein-level confirmation is

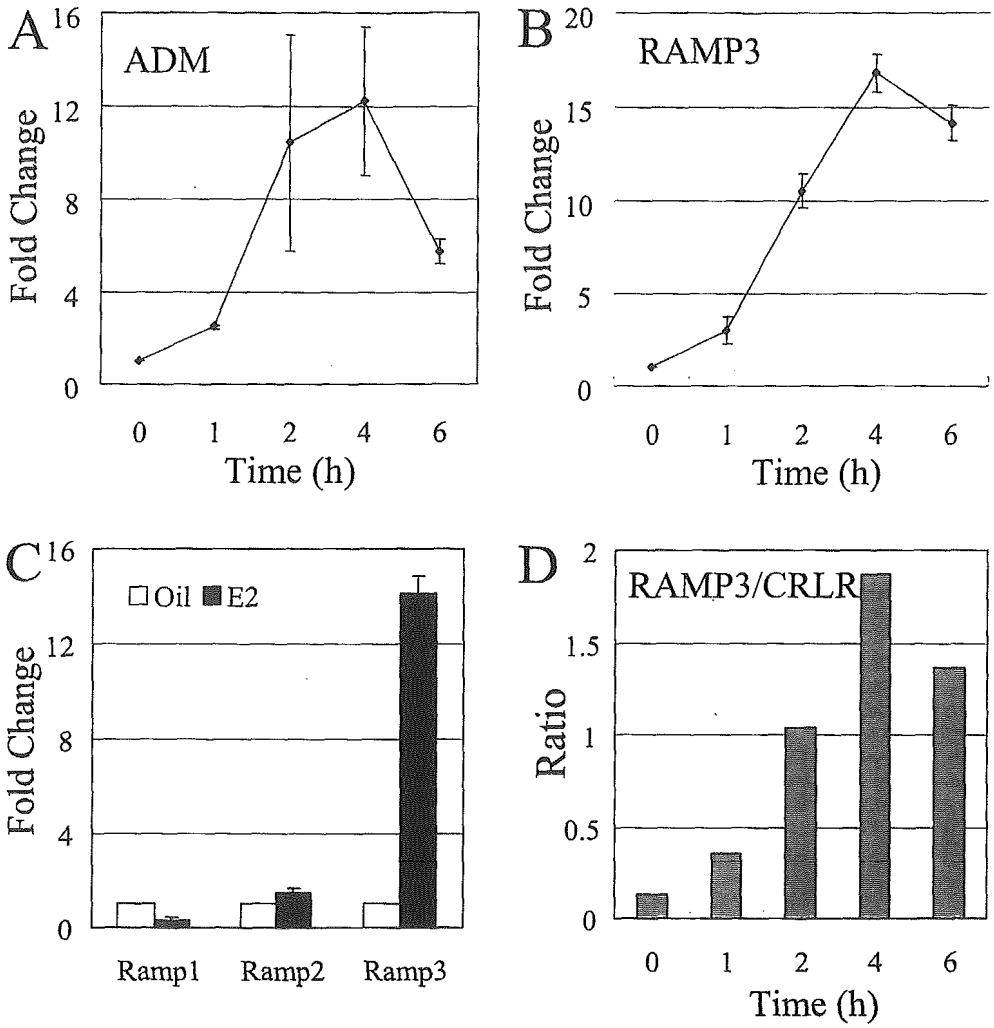

Figure 2 Temporal changes in ADM and RAMP3 gene expression. Ovariectomized mice were injected with 5 μg/kg b.w. estradiol and total uterine RNA was isolated 1, 2, 4 and 6 h later. ADM (A) and RAMP3 (B) gene-expression levels were estimated by quantitative PCR. Shown is the change in expression over time relative to the gene-expression level at 0 h (fold change). Uterine RNA was prepared from three independent experiments and average fold changes and errors are indicated. The *x* axes indicate the time after estrogen administration while the *y* axes indicate fold changes in gene expression. (C) Of the different RAMP genes, only RAMP3 was strongly activated by estradiol. Total uterine RNA was isolated 6 h after injecting 5 μg/kg b.w. estradiol and the change in RAMP gene expression relative to expression in the sesame-oil-injected control uteri was estimated by quantitative PCR. Uterine RNA was prepared from three independent experiments and the average fold changes and errors are indicated. (D) Gene expression of RAMP3 relative to CRLR expression mRNA after estradiol administration was determined by quantitative PCR. The ratio of RAMP3 mRNA to CRLR mRNA was calculated on the basis of the copy numbers of RAMP3 and CRLR mRNA. Approximately equal amounts of mRNA were detected 2 h after estrogen administration. The *x* axis indicates time after estrogen administration while the *y* axis indicates the ratio of RAMP3 mRNA to CRLR mRNA. E2, 17β-estradiol.

essential, the rapid increase of RAMP3 mRNA may affect the properties of the ADM receptor and it appears that the net effect of estrogen exposure is to convert existing CRLR protein into an ADM receptor.

The ER binds to the promoter region of the ADM and RAMP3 genes

Since ADM expression is induced early after estrogen administration, we examined whether the ADM gene

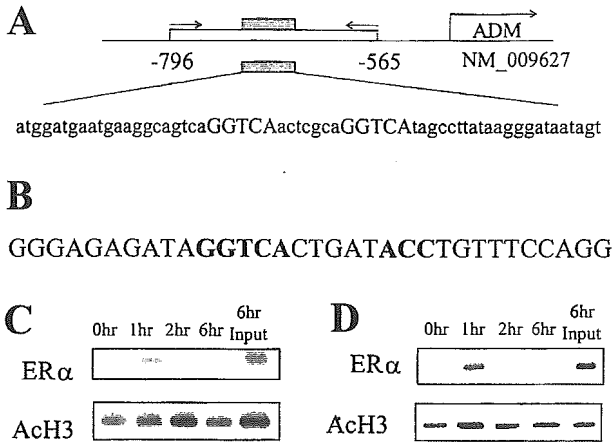

Figure 3 Chromatin immunoprecipitation of the ADM promoter region. (A) Schematic diagram of the ADM promoter region. The ADM gene is indicated on the right. The putative ERE is indicated by a black box. The nucleotide sequence containing the two direct repeats is indicated (the repeats are indicated by capital letters). (B) The open box indicates the region amplified by PCR. The nucleotide sequence of RAMP3 intron containing the putative ERE is indicated (the motif is highlighted in bold). (C) The ADM promoter region was precipitated by anti-ERα antibody. Chromatin immunoprecipitation was performed on mouse uteri obtained 0, 1, 2 and 6 h after treatment with 5 μg/kg b.w. estradiol. At 1 and 2 h after estrogen administration, the ADM promoter region was precipitated by anti-ERα (upper panel). When chromatin immunoprecipitation using anti-acetylated histone H3 (AcH3) antibody was performed, the ADM promoter region was precipitated both before and after estrogen administration (lower panel). Without specific antibodies, no DNA was amplified (data not shown). (D) The RAMP3 intron was precipitated by anti-ERα antibody. Chromatin immunoprecipitation was performed on mouse uteri obtained 0, 1, 2 and 6 h after treatment with 5 μg/kg b.w. estradiol. At 1 h after estrogen administration, the RAMP3 intron was precipitated by anti-ERα (upper panel). When chromatin immunoprecipitation using anti-acetylated histone H3 antibody was performed, the same region was precipitated both before and after estrogen administration (lower panel). Without specific antibodies, no DNA was amplified (data not shown).

can be directly activated by the ER. Analysis of the sequence upstream of the ADM gene revealed direct repeats of the canonical ERE motif between positions −744 and −748 and between positions −756 and −760 from the 5′ end of the ADM gene (NM_009627; Fig. 3A). [The actual distance from the transcriptional start site may differ since the transcriptional start site database (http://dbtss/hgc/jp/) showed that the ADM gene has multiple transcriptional start sites located between positions −9 and −14.] To examine whether the ER can bind to the element *in vivo*, we performed chromatin-immunoprecipitation assays with uterine DNA obtained 0, 1, 2 and 6 h after treatment with 5 μg/kg b.w. estradiol. A DNA fragment containing the direct repeats was precipitated by the anti-ERα antibody only after estrogen administration (Fig. 3C), suggesting that the ER binds to the promoter region of the ADM gene and activates its transcription. Unlike the ligand-dependent binding of the ER to the ADM promoter, anti-acetylated histone H3 antibody precipitated the direct repeat-bearing DNA fragment even before estrogen was added (0 h). Thus the chromatin structure of the ADM gene is open before the addition of ligand and is accessible to the ER when the ligand is administered. Similarly RMAP3 expression was also activated by estrogen. Although ERE could not be found near the transcription start site, a putative ERE was found in the first intron of RAMP3 gene (13 620 bp from the 5′ end of the first intron; Fig. 3B). Chromatin immunoprecipitation confirmed that the DNA fragment containing the putative ERE could be precipitated by anti-ERα only when estrogen was administered (Fig. 3D). Similar to ADM gene, anti-acetylated histone H3 antibody could precipitate the DNA fragment of RAMP3 even before estrogen administration.

The ADM gene is expressed in uterine stroma cells

To examine the location of ADM gene expression in the uterus, we used *in situ* hybridization to detect ADM mRNA in uteri obtained 6 h after stimulation with 5 μg/kg b.w. estrogen. ADM mRNA was mainly detected in the endometrial stroma (Fig. 4). In contrast to the weak signal in unstimulated ovariectomized uteri, the ADM gene was strongly expressed in the stroma of the estrogen-stimulated uteri. Thus estrogen induces ADM gene expression in the stroma only. Interestingly, the ADM gene was not expressed in the myometrium or epithelial cells. A similar expression pattern was observed for RAMP3, namely weak expression in unstimulated uteri and strong expression in the stroma of estrogen-stimulated uteri. The distribution of RAMP3 mRNA in the stroma was similar to that of CRLR mRNA (data not shown). In contrast, RAMP2 expression did not change after estrogen administration, although its expression was limited to the stroma. Thus the temporal (Fig. 2) and spatial (Fig. 4) expression of the ADM and RAMP3 genes correlated closely.

ADM gene is not activated in ERα-null mice

To examine whether ADM gene activation is dependent on ER, we examined the gene-expression profile of ERα and -β-null mice using DNA microarray. As shown in Fig. 5, ADM was activated in wild-type and ERβ-null mice but not ERα-null mice. This result confirmed that ERα is responsible for the gene activation of ADM. Similarly, RAMP3 was also activated in wild-type and ERβ-null mice but not ERα-null mice. These results suggest that both ADM and RAMP3 genes are regulated by ERα but not ERβ.

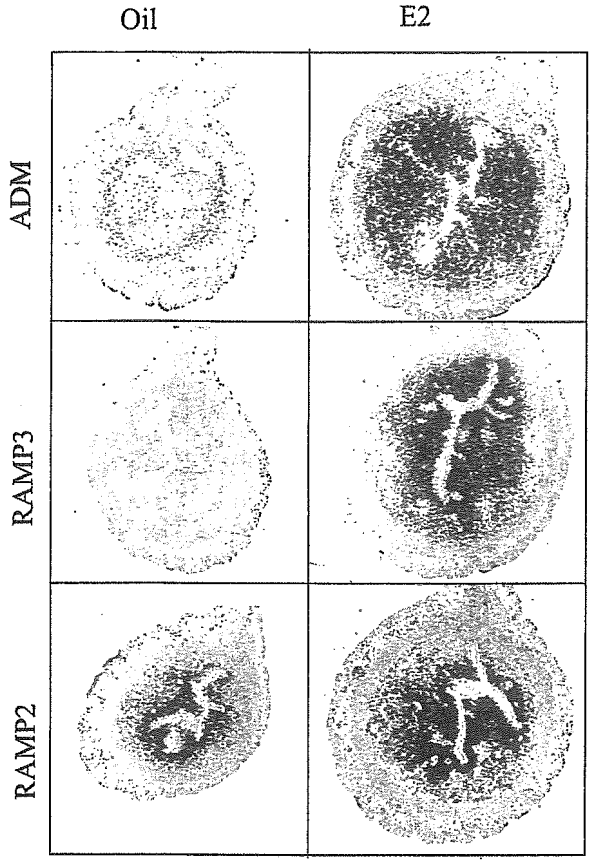

Figure 4 Distribution of ADM, RAMP3 and CRLR mRNAs in estrogen-treated uteri. Ovariectomized mice were given 5 μg/kg b.w. estradiol and their uteri were isolated 6 h later. ADM, RAMP3 and CRLR gene expression was examined by *in situ* hybridization. As a control, mice were injected with sesame oil. The dark-field images were converted to red and merged with bright-field images. E2, 17β-estradiol.

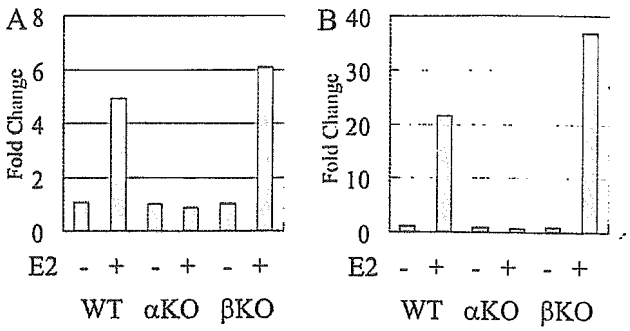

Figure 5 ADM and RAMP3 genes are not activated in ERα-null mice. Female C57BL/6J mice and ERα- and -β-null mice were ovariectomized at 8 weeks of age and injected with either 17β-estradiol (E2, +; 50 μg/kg body weight) or vehicle (−) at 10 weeks of age. The whole uteri were collected 6 h later, and the gene-expression profile was analyzed by DNA microarray. Calculated fold changes are indicated. (A) ADM, (B) RAMP3. WT, wild type; αKO, ERα-knockout; βKO, ERβ-knockout.

Discussion

Since the development of DNA microarray technology, many genes have been listed as being responsive to specific stimuli. However, despite knowing which genes may be activated or repressed by a particular stimulus, the biological significance of this information is still largely lacking. Moreover, many genes identified by DNA microarray analysis have not been validated to respond to the stimulus in question by other methods. In this study, we focused on ADM and RAMP3 genes that were shown by DNA microarray analysis to be activated by estrogen and showed that the ADM and RAMP3 genes are directly regulated by the ER.

ADM was originally identified as a potent vasorelaxant peptide that is produced by pheochromocytoma cells (Kitamura *et al.* 1993*b*). The human form consists of 52 amino acid residues and the mouse and rat forms consist of 50 amino acid residues (Sakata *et al.* 1993). Subsequent studies revealed that ADM is expressed not only in vascular endothelial cells but also in the adrenal gland (Kitamura *et al.* 1993*a*), kidney (Kitamura *et al.* 1993*a*), heart (Perret *et al.* 1993), bone (Cornish *et al.* 1997) and other tissues. Thus ADM is active in the cardiovascular system (Ishiyama *et al.* 1993), the endocrine system (Yamaguchi *et al.* 1995) and the central nervous system (Wang *et al.* 1995). It is also known to be expressed in the reproductive system as its expression in the uterus has been observed; moreover, uterine ADM expression increases during pregnancy (Di Iorio *et al.* 1999, Michishita *et al.* 1999, Thota *et al.* 2003, Upton *et al.* 1997). Furthermore, studies of the relationship between estrogen and ADM expression in the uterus have revealed a positive correlation between estrogen levels and ADM gene expression (Cameron *et al.* 2002, Ikeda *et al.* 2004, Jerat & Kaufman 1998). Thus ADM appears to participate in phyiological processes affecting the uterus.

Many studies on ADM are mainly concerned with its long-lasting activity in physiological processes such as hypotension (Kitamura *et al.* 1995), bone development (Cornish *et al.* 2003) and gestation (Thota *et al.* 2003, Upton *et al.* 1997). With regard to the reproductive system, ADM has been reported to generally act as a relaxant or vasodilator (Makino *et al.* 1999, Yanagita *et al.* 2000). However, the data presented in this paper show that locally expressed ADM can also function in the uterus in a more transient manner, since estrogen-induced ADM gene expression in the uterus only occurs in the stroma over a short period. Interestingly, although ADM, RAMP3 and CRLR are only expressed in the stromal cells, this kind of local effect of ADM has been observed in many tissues (Kato *et al.* 1997, Martinez *et al.* 1997, Nishimura *et al.* 1997, Seguchi *et al.* 1995, Takahashi *et al.* 1997), including the

uterus (Nikitenko *et al.* 2000). Further analysis of ADM signaling is needed to clarify the effects of estrogen on uterine growth.

In the present study, we also demonstrated by chromatin-immunoprecipitation assays that the ADM promoter is recognized by the ER in a ligand (estrogen)-dependent manner. Although we used whole uteri for this analysis, these results appear to reflect the effects of ADM in the stroma, which is abundant in the uterus. Our data show that rapid binding of the ER directly to the ADM promoter may be important for ADM gene activation. A putative ERE was also detected in the RAMP3 gene, though it was found in the first intron of the gene. Chromatin immunoprecipitation confirmed that this region could be recognized by ERα in a ligand-dependent manner.

In summary we have shown that ADM and RAMP3 are genes that are directly activated by the ER, and that ADM and RAMP3 are directly recognized by the ERα. Similarities between the gene-activation patterns of ADM and RAMP3 suggest that a combination of RAMP3 and CRLR functions as an ADM receptor after estrogen administration. Although functional analysis of these genes is essential, the early activation of ADM after estrogen administration suggests that ADM plays important roles in the reproductive system in different ways: first, in processes such as pregnancy, where its involvement and expression are prolonged (Di Iorio *et al.* 1999, Michishita *et al.* 1999, Thota *et al.* 2003, Upton *et al.* 1997), and second, in processes such as estrogen-induced uterine growth, where its involvement and expression are transient.

Acknowledgements

This work was supported in part by a Core Research for Evolutional Science research grant from the Japan Science and Technology Cooperation, a Grant-in-Aid for Scientific Research from the Japan Society for the Promotion of Science, a Grant-in-Aid for Scientific Research from the Ministry of Education, Science, Sports and Culture of Japan, a Health Sciences Research Grant from the Ministry of Health, Labour and Welfare of Japan, a research grant from the Ministry of Environment, Japan, and a research grant from New Energy and Industrial Technology Development Organization (NEDO). The authors declare that there is no conflict of interest that would prejudice the impartiality of this scientific work.

References

Cameron VA, Autelitano DJ, Evans JJ, Ellmers LJ, Espiner EA, Nicholls MG & Richards AM 2002 Adrenomedullin expression in rat uterus is correlated with plasma estradiol. *American Journal of Physiology Endocrinology & Metabolism* **282** E139–E146.

Cornish J, Callon KE, Coy DH, Jiang NY, Xiao L, Cooper GJ & Reid IR 1997 Adrenomedullin is a potent stimulator of osteoblastic activity in vitro and in vivo. *American Journal of Physiology Endocrinology & Metabolism* **273** E1113–E1120.

Cornish J, Naot D & Reid IR 2003 Adrenomedullin–a regulator of bone formation. *Regulatory Peptides* **112** 79–86.

Di Iorio R, Marinoni E, Letizia C, Villaccio B, Alberini A & Cosmi EV 1999 Adrenomedullin production is increased in normal human pregnancy. *European Journal of Endocrinology* **140** 201–206.

Dupont S, Krust A, Gansmuller A, Dierich A, Chambon P & Mark M 2000 Effect of single and compound knockouts of estrogen receptors alpha (ERalpha) and beta (ERbeta) on mouse reproductive phenotypes. *Development* **127** 4277–4291.

Ikeda K, Arao Y, Otsuka H, Kikuchi A & Kayama F 2004 Estrogen and phytoestrogen regulate the mRNA expression of adrenomedullin and adrenomedullin receptor components in the rat uterus. *Molecular & Cell Endocrinology* **223** 27–34.

Ishiyama Y, Kitamura K, Ichiki Y, Nakamura S, Kida O, Kangawa K & Eto T 1993 Hemodynamic effects of a novel hypotensive peptide, human adrenomedullin, in rats. *European Journal of Pharmacology* **241** 271–273.

Jerat S & Kaufman S 1998 Effect of pregnancy and steroid hormones on plasma adrenomedullin levels in the rat. *Canadian Journal of Physiology & Pharmacology* **76** 463–466.

Kato H, Shichiri M, Marumo F & Hirata Y 1997 Adrenomedullin as an autocrine/paracrine apoptosis survival factor for rat endothelial cells. *Endocrinology* **138** 2615–2620.

Kitamura K, Kangawa K, Matsuo H & Eto T 1995 Adrenomedullin. Implications for hypertension research. *Drugs* **49** 485–495.

Kitamura K, Sakata J, Kangawa K, Kojima M, Matsuo H & Eto T 1993*a* Cloning and characterization of cDNA encoding a precursor for human adrenomedullin. *Biochemical & Biophysics Research Communications* **194** 720–725.

Kitamura K, Kangawa K, Kawamoto M, Ichiki Y, Nakamura S, Matsuo H & Eto T 1993*b* Adrenomedullin: a novel hypotensive peptide isolated from human pheochromocytoma. *Biochemistry & Biophysics Research Communications* **192** 553–560.

Makino I, Shibata K, Makino Y, Kangawa K & Kawarabayashi T 1999 Adrenomedullin attenuates the hypertension in hypertensive pregnant rats induced by N(G)-nitro-L-arginine methyl ester. *European Journal of Pharmacology* **371** 159–167.

Martinez A, Miller MJ, Catt KJ & Cuttitta F 1997 Adrenomedullin receptor expression in human lung and in pulmonary tumors. *Journal of Histochemistry & Cytochemistry* **45** 159–164.

McLatchie LM, Fraser NJ, Main MJ, Wise A, Brown J, Thompson N, Solari R, Lee MG & Foord SM 1998 RAMPs regulate the transport and ligand specificity of the calcitonin-receptor-like receptor. *Nature* **393** 333–339.

Michishita M, Minegishi T, Abe K, Kangawa K, Kojima M, Ibuki Y, Upton PD, Austin C, Taylor GM, Nandha KA *et al.* 1999 Expression of adrenomedullin (ADM) and its binding sites in the rat uterus: increased number of binding sites and ADM messenger ribonucleic acid in 20-day pregnant rats compared with nonpregnant rats. *Obstetics & Gynecology* **93** 66–70.

Nikitenko LL, MacKenzie IZ, Rees MC & Bicknell R 2000 Adrenomedullin is an autocrine regulator of endothelial growth in human endometrium. *Molecular & Human Reproduction* **6** 811–819.

Nishimura J, Seguchi H, Sakihara C, Kureishi Y, Yoshimura H, Kobayashi S & Kanaide H 1997 The relaxant effect of adrenomedullin on particular smooth muscles despite a general expression of its mRNA in smooth muscle, endothelial and epithelial cells. *British Journal of Pharmacology* **120** 193–200.

Perret M, Broussard H, LeGros T, Burns A, Chang JK, Summer W, Hyman A & Lippton H 1993 The effect of adrenomedullin on the isolated heart. *Life Science* **53** PL377–PL379.

Sakata J, Shimokubo T, Kitamura K, Nakamura S, Kangawa K, Matsuo H & Eto T 1993 Molecular cloning and biological activities of rat adrenomedullin, a hypotensive peptide. *Biochemistry & Biophysics Research Communications* **195** 921–927.

Seguchi H, Nishimura J, Kobayashi S, Kumazawa J & Kanaide H 1995 Autocrine regulation of the renal arterial tone by adrenomedullin. *Biochemistry & Biophysics Research Communications* **215** 619–625.

Szego CM & Davis JS 1967 Adenosine 3′,5′-monophosphate in rat uterus: acute elevation by estrogen. *PNAS* **58** 1711–1718.

Takahashi K, Satoh F, Sone M, Murakami O, Sasano H, Mouri T & Shibahara S 1997 Expression of adrenomedullin mRNA in the human brain and pituitary. *Peptides* **18** 1051–1053.

Thota C, Gangula PR, Dong YL & Yallampalli C 2003 Changes in the expression of calcitonin receptor-like receptor, receptor activity-modifying protein (RAMP) 1, RAMP2, and RAMP3 in rat uterus during pregnancy, labor, and by steroid hormone treatments. *Biology of Reproduction* **69** 1432–1437.

Upton PD, Austin C, Taylor GM, Nandha KA, Clark AJ, Ghatei MA, Bloom SR & Smith DM 1997 Expression of adrenomedullin (ADM) and its binding sites in the rat uterus: increased number of binding sites and ADM messenger ribonucleic acid in 20-day pregnant rats compared with nonpregnant rats. *Endocrinology* **138** 2508–2514.

Wang X, Yue TL, Barone FC, White RF, Clark RK, Willette RN, Sulpizio AC, Aiyar NV, Ruffolo RR Jr & Feuerstein GZ 1995 Discovery of adrenomedullin in rat ischemic cortex and evidence for its role in exacerbating focal brain ischemic damage. *PNAS* **92** 11480–11484.

Watanabe H, Suzuki A, Mizutani T, Khono S, Lubahn DB, Handa H & Iguchi T 2002 Genome-wide analysis of changes in early gene expression induced by oestrogen. *Genes Cells* **7** 497–507.

Watanabe H, Suzuki A, Kobayashi M, Lubahn DB, Handa H & Iguchi T 2003 Similarities and differences in uterine gene expression patterns caused by treatment with physiological and non-physiological estrogens. *Journal of Molecular Endocrinology* **31** 487–497.

Yamaguchi T, Baba K, Doi Y & Yano K 1995 Effect of adrenomedullin on aldosterone secretion by dispersed rat adrenal zona glomerulosa cells. *Life Science* **56** 379–387.

Yanagita T, Yamamoto R, Sugano T, Kobayashi H, Uezono Y, Yokoo H, Shiraishi S, Minami SI & Wada A 2000 Adrenomedullin inhibits spontaneous and bradykinin-induced but not oxytocin- or prostaglandin F(2 alpha)-induced periodic contraction of rat uterus. *British Journal of Pharmacology* **130** 1727–1730.

Zor U, Koch Y, Lamprecht SA, Ausher J & Lindner HR 1973 Mechanism of oestradiol action on the rat uterus: independence of cyclic AMP, prostaglandin E2 and beta-adrenergic mediation. *Journal of Endocrinology* **58** 525–533.

Received 26 July 2005
Accepted 17 October 2005

Differential contributions of Mesp1 and Mesp2 to the epithelialization and rostro-caudal patterning of somites

Yu Takahashi[1,*], Satoshi Kitajima[1], Tohru Inoue[1], Jun Kanno[1] and Yumiko Saga[2,*]

[1]Cellular & Molecular Toxicology Division, National Institute of Health Sciences, 1-18-1 Kamiyoga, Setagayaku, Tokyo 158-8501, Japan
[2]Division of Mammalian Development, National Institute of Genetics, Yata 1111, Mishima 411-8540, Japan
*Authors for correspondence (e-mail: yutak@nihs.go.jp and ysaga@lab.nig.ac.jp)

Accepted 29 November 2004

Development 132, 787-796
Published by The Company of Biologists 2005
doi:10.1242/dev.01597

Summary

Mesp1 and Mesp2 are homologous basic helix-loop-helix (bHLH) transcription factors that are co-expressed in the anterior presomitic mesoderm (PSM) just prior to somite formation. Analysis of possible functional redundancy of Mesp1 and Mesp2 has been prevented by the early developmental arrest of Mesp1/Mesp2 double-null embryos. Here we performed chimera analysis, using either Mesp2-null cells or Mesp1/Mesp2 double-null cells, to clarify (1) possible functional redundancy and the relative contributions of both Mesp1 and Mesp2 to somitogenesis and (2) the level of cell autonomy of Mesp functions for several aspects of somitogenesis. Both Mesp2-null and Mesp1/Mesp2 double-null cells failed to form initial segment borders or to acquire rostral properties, confirming that the contribution of Mesp1 is minor during these events. By contrast, Mesp1/Mesp2 double-null cells contributed to neither epithelial somite nor dermomyotome formation, whereas Mesp2-null cells partially contributed to incomplete somites and the dermomyotome. This indicates that Mesp1 has a significant role in the epithelialization of somitic mesoderm. We found that the roles of the Mesp genes in epithelialization and in the establishment of rostral properties are cell autonomous. However, we also show that epithelial somite formation, with normal rostro-caudal patterning, by wild-type cells was severely disrupted by the presence of Mesp mutant cells, demonstrating non-cell autonomous effects and supporting our previous hypothesis that Mesp2 is responsible for the rostro-caudal patterning process itself in the anterior PSM, via cellular interaction.

Key words: Somitogenesis, Epithelial-mesenchymal conversion, Mesp2, Chimera analysis, Mouse

Introduction

Somitogenesis is not only an attractive example of metameric pattern formation but is also a good model system for the study of morphogenesis, particularly epithelial-mesenchymal interconversion in vertebrate embryos (Gossler and Hrabe de Angelis, 1997; Pourquié, 2001). The primitive streak, or tailbud mesenchyme, supplies the unsegmented paraxial mesoderm, known as presomitic mesoderm (PSM). Mesenchymal cells in the PSM undergo mesenchymal-epithelial conversion to form epithelial somites in a spatially and temporally coordinated manner. Somites then differentiate, in accordance with environmental cues from the surrounding tissues, into dorsal epithelial dermomyotome and ventral mesenchymal sclerotome (Borycki and Emerson, 2000; Fan and Tessier Lavigne, 1994). Hence, the series of events that occur during somitogenesis provide a valuable example of epithelial-mesenchymal conversion. The dermomyotome gives rise to both dermis and skeletal muscle, whereas the sclerotome forms cartilage and bone in both the vertebrae and the ribs. Each somite is subdivided into two compartments, the rostral (anterior) and caudal (posterior) halves. This rostro-caudal polarity appears to be established just prior to somite formation (Saga and Takeda, 2001).

Mesp1 and Mesp2 are closely related members of the basic helix-loop-helix (bHLH) family of transcription factors but share significant sequence homology only in their bHLH regions (Saga et al., 1996; Saga et al., 1997). During development of the mouse embryo, both *Mesp1* and *Mesp2* are specifically expressed in the early mesoderm just after gastrulation and in the paraxial mesoderm during somitogenesis. Mesp1/Mesp2 double-null embryos show defects in early mesodermal migration and thus fail to form most of the embryonic mesoderm, leading to developmental arrest (Kitajima et al., 2000). Mesp1-null embryos exhibit defects in single heart tube formation, due to a delay in mesodermal migration, but survive to the somitogenesis stage (Saga et al., 1999), suggesting that there is some functional redundancy, i.e. compensatory functions of Mesp2 in early mesoderm. During somitogenesis, both *Mesp1* and *Mesp2* are expressed in the anterior PSM just prior to somite formation. Although we have shown that Mesp2, but not Mesp1, is essential for somite formation and the rostro-caudal patterning of somites (Saga et al., 1997), a possible functional redundancy between Mesp1 and Mesp2 has not yet been clearly established.

To further clarify the contributions of Mesp1 and Mesp2 to somitogenesis, analysis of Mesp1/Mesp2 double-null embryos

is necessary, but because of the early mesodermal defects already described, these knockout embryos lack a paraxial mesoderm, which prevents any analysis of somitogenesis. We therefore adopted a strategy that utilized chimera analysis. As we have reported previously, the early embryonic lethality of a Mesp1/Mesp2 double knockout is rescued by the presence of wild-type cells in a chimeric embryo, but the double-null cells cannot contribute to the cardiac mesoderm (Kitajima et al., 2000). This analysis, however, focused only on early heart morphogenesis and did not investigate the behavior of Mesp1/Mesp2 double-null cells in somitogenesis. In this report, we focus upon somitogenesis and compare two types of chimeras using either Mesp1/Mesp2 double-null cells or Mesp2-null cells to investigate Mesp1 function during somitogenesis.

Another purpose of our chimera experiments was to elucidate the cell autonomy of Mesp functions. In the process of somite formation, mesenchymal cells in the PSM initially undergo epithelialization at the future segment boundary, independently of the already epithelialized dorsal or ventral margin of the PSM (Sato et al., 2002). Epithelial somite formation is disrupted in the Mesp2-null embryo, indicating that Mesp2 is required for epithelialization at the segment boundary. Although Mesp products are nuclear transcription factors and their primary functions must therefore be cell autonomous (transcriptional control of target genes), it is possible that the roles of Mesp2 in epithelialization are mediated by the non-cell autonomous effects of target genes. We therefore asked whether the defects in Mesp2-null cells during epithelialization could be rescued by the presence of surrounding wild-type cells. Additionally, we would expect to find that the role of Mesp2 in establishing rostro-caudal polarity is rescued in a similar way.

Our analysis suggests that Mesp1 and Mesp2 have redundant functions and are both cell-autonomously involved in the epithelialization of somitic mesoderm. In addition, our results highlight some non-cell autonomous effect of Mesp2-null and Mesp1/Mesp2-null cells.

Materials and methods

Generation of chimeric embryos

As described previously (Kitajima et al., 2000), chimeric embryos were generated by aggregating 8-cell embryos of wild-type mice (ICR) with those of mutant mice that were genetically marked with the *ROSA26* transgene (Zambrowicz et al., 1997). Mesp1/Mesp2 double-null embryos were generated by crossing *wko-del (+/–)* and *Mesp1(+/–)/Mesp2(+/cre)* mice as described previously (Kitajima et al., 2000). This strategy enables us to distinguish chimeric embryos derived from homozygous embryos, which have two different mutant alleles, from those derived from heterozygous embryos. Likewise, Mesp2-null embryos were generated by crossing *P2v1(+/–)* mice (Saga et al., 1997) and *P2GFP (+/gfp)* mice (Y.S. and S.K., unpublished) that were also labeled with the *ROSA26* locus. The genotype of the chimeric embryos was determined by PCR using yolk sac DNA.

Histology, histochemistry and gene expression analysis

The chimeric embryos were fixed at 11 days postcoitum (dpc) and stained in X-gal solution for the detection of β-galactosidase activity, as described previously (Saga et al., 1999). For histology, samples stained by X-gal were postfixed with 4% paraformaldehyde, dehydrated in an ethanol series, embedded in plastic resin (Technovit 8100, Heraeus Kulzer) and sectioned at 3 μm. The methods used for gene expression analysis by in-situ hybridization of whole-mount samples and frozen sections and skeletal preparation by Alcian Blue/Alizarin Red staining were described previously (Saga et al., 1997; Takahashi et al., 2000). Probes for in-situ hybridization for *Uncx4.1* (Mansouri et al., 1997; Neidhardt et al., 1997), *Delta-like 1 (Dll1)* (Bettenhausen et al., 1995) and *Paraxis* (Burgess et al., 1995) were kindly provided by Drs Peter Gruss, Achim Gossler and Alan Rawls, respectively. A probe for *EphA4* (Nieto et al., 1992) was cloned by PCR. For detection of actin filaments, frozen sections were stained with AlexaFluor 488-conjugated phalloidin (Molecular Probes) according to the manufacturer's protocol.

Results

Possible functional redundancy and different contributions of Mesp1 and Mesp2 in somitogenesis

During somitogenesis, both *Mesp1* and *Mesp2* are expressed in the anterior PSM just prior to somite formation and their expression domains overlap (Fig. 1A). Mesp1-null embryos form morphologically normal somites and show normal rostro-caudal patterning within each somite (Fig. 1B,E-H), indicating that Mesp1 is not essential for somitogenesis. By contrast, Mesp2 is essential for both the formation and rostro-caudal patterning of somites, as Mesp2-null embryos have no epithelial somites and lose rostral half properties, resulting in caudalization of the entire somitic mesoderm (Saga et al., 1997) (Fig. 1C,D).

Although somite formation and rostro-caudal patterning is disrupted in the Mesp2-null embryo, histological differentiation into dermomyotome and sclerotome is not affected. It is noteworthy that the Mesp2-null embryo still forms disorganized dermomyotomes without forming epithelial somites (Saga et al., 1997). As *Mesp1* is expressed at normal levels in the PSM of Mesp2-null embryos (Fig. 1C,D), it is possible that Mesp1 functions to rescue some aspects of somitogenesis in the Mesp2-null embryo. In order to further clarify the contributions of both Mesp1 and Mesp2 during somitogenesis, we therefore generated chimeric embryos with either Mesp2-null cells or Mesp1/Mesp2 double-null cells and compared the behavior of mutant cells during somitogenesis (Fig. 2).

Mesp2-null cells tend to be eliminated from the epithelial somite and the dermomyotome, but can partially contribute to both of these structures

We first generated Mesp2-null chimeric embryos (*Mesp2*$^{-/-}$ with *Rosa26*: wild) to analyze cell autonomy of Mesp2 function during somitogenesis. The control chimeric embryo (*Mesp2*$^{+/-}$ with *Rosa26*: wild) showed normal somitogenesis and a random distribution of X-gal stained cells (Fig. 3A). The Mesp2-null chimeric embryos formed abnormal somites that exhibited incomplete segmentation (Fig. 3B), but histological differentiation of dermomyotome and sclerotome was observed. Within the incomplete somite, X-gal-stained Mesp2-null cells were mainly localized in the rostral and central regions, surrounded by wild-type cells at the dorsal, ventral and caudal sides (Fig. 3B). The surrounding wild-type cells, however, did not form an integrated epithelial sheet, but consisted of several epithelial cell clusters. Such trends were more obviously observed in other sections, where wild-type cells were found to form multiple small epithelial clusters (Fig.

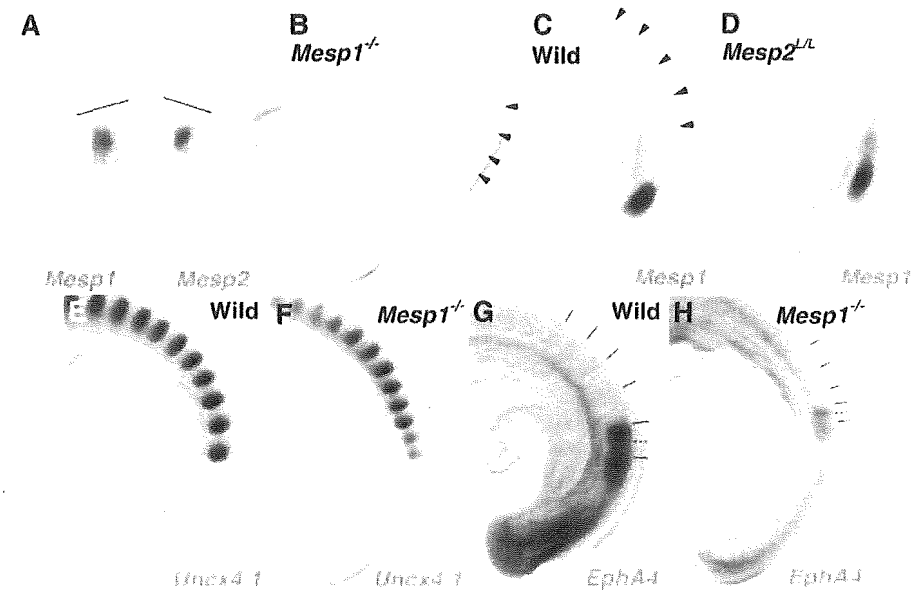

Fig. 1. *Mesp1* and *Mesp2* are co-expressed in the anterior PSM but have differing roles in somitogenesis. (A) Overlapping expression of *Mesp1* and *Mesp2* is revealed by in-situ hybridization using the left and right halves of the same embryo. The lines show most recently formed somite boundaries. (B-C) A Mesp1-null embryo (B) shows the same normal somite formation as a wild-type embryo (C). Arrowheads indicate somite boundaries. (D) In Mesp2-null embryos, no somite formation is observed but *Mesp1* is expressed at comparable levels to wild type, although its expression is anteriorly extended and blurred. (E-H) Mesp1-null embryos show normal rostro-caudal patterning of somites. (E,F) Expression of a caudal half marker, *Uncx4.1*. (G,H) Expression of a rostral half marker, *EphA4*. The lines indicate presumptive or formed somite boundaries and the dotted line indicates approximate position of somite half boundary.

3C,D). Mesp2-null cells tended to be eliminated from the epithelial clusters, although they were partially integrated into these structures (blue arrows in Fig. 3C,D). Likewise, small numbers of Mesp2-null cells were found to contribute to the dermomyotome (Fig. 3E,F). Mesp2-null cells also appeared to form the major part of the sclerotome.

Mesp2 is required for the cell-autonomous acquisition of rostral properties

We have previously demonstrated that suppression by Mesp2

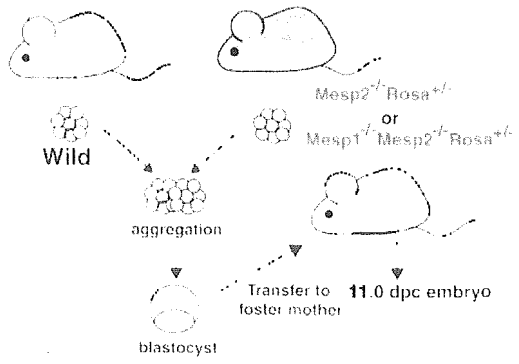

Fig. 2. Schematic representation of chimera analysis method. Either Mesp2-null or Mesp1/Mesp2 double-null embryos, genetically labeled with *Rosa* locus, were aggregated with wild-type embryos at the 8-cell stage, and the resulting chimeras were subjected to analysis at 11.0 dpc.

of the caudal genes *Dll1* and *Uncx4.1* in presumptive rostral half somites is a crucial event in the establishment of the rostro-caudal pattern of somites (Saga et al., 1997; Takahashi et al., 2000). As Mesp2-null embryos exhibit caudalization of somites, Mesp2-null cells are predicted to be unable to express rostral properties. Hence, Mesp2-null cells are expected to distribute to the caudal region of each somite where the rostro-caudal patterns are rescued by wild-type cells in a chimeric embryo. In this context, the localization of Mesp2-null cells at the rostral side was an unexpected finding. We interpret this to mean that the rostral location of Mesp2-null cells is due to a lack of epithelialization functions (see Discussion).

To examine rostro-caudal properties in Mesp2-null cells, located in the rostral side, we analyzed the expression of a caudal half marker gene, *Uncx4.1* (Mansouri et al., 1997; Neidhardt et al., 1997). Analysis of adjacent sections revealed that *lacZ*-expressing Mesp2-null cells, localized at the rostral and central portion, ectopically expressed *Uncx4.1* (Fig. 4A-D). This strongly suggests that Mesp2-null cells cannot acquire rostral properties even if surrounded by wild-type cells, and that Mesp2 function is cell-autonomously required for the acquisition of rostral properties. We also observed that the small number of Mesp2-null cells distributed mostly to the caudal end of the dermomyotome (Fig. 3E,F) and that the expression pattern of *Uncx4.1* was normal in the dermomyotome (Fig. 4E,F). In the sclerotome, *lacZ*-expressing Mesp2-null cells often distributed to the rostral side, where expression of *Uncx4.1* was abnormally elevated (Fig. 4G,H). The vertebrae of the Mesp2-null chimeric fetus showed a partial fusion of the neural arches, which was reminiscent of

Mesp2-hypomorphic fetuses (Fig. 4I,J) (Nomura-Kitabayashi et al., 2002). Fusion of proximal rib elements was also observed (Fig. 4K,L).

Mesp1/Mesp2 double-null cells cannot contribute to the formation of epithelial somites or to the dermomyotome

To address the question of whether Mesp1, in addition to Mesp2, exhibits any function during somitogenesis, we next generated Mesp1/Mesp2 double-null chimeric embryos and compared them with the Mesp2-null chimeric embryos described in the previous sections. We first performed whole-mount X-gal staining of embryos at 11 dpc. In the control chimeric embryo, the X-gal-stained Mesp1/Mesp2 double-heterozygous cells distributed randomly throughout the embryonic body, including the somite region (Fig. 5A,C). By contrast, the Mesp1/Mesp2 double-null chimeric embryo displayed a strikingly uneven pattern of cellular distribution in the somite region. The X-gal stained Mesp1/Mesp2 double-null cells were localized at the medial part of embryonic tail and were not observed in the lateral part of the somite region (Fig. 5B,D). Histological examination of parasagittal sections further revealed obvious differences in the cellular contribution to somite formation (Fig. 5E,F). In the control chimeric embryo, Mesp1/Mesp2 double-heterozygous cells distributed randomly throughout the different stages of somitogenesis (PSM, somite, dermomyotome and sclerotome: Fig. 5E). In the Mesp1/Mesp2 double-null chimeric embryo, neither the initial segment border nor epithelial somites were formed, but histologically distinguishable dermomyotome-like and sclerotome-like compartments were generated (Fig. 5F). In addition, Mesp1/Mesp2 double-null cells and wild-type cells were randomly mixed in the PSM, whereas the dermomyotome-like epithelium consisted exclusively of wild-type cells and the sclerotome-like compartment consisted mostly of Mesp1/Mesp2 double-null cells. This suggests that either Mesp1 or Mesp2 is cell-autonomously required for the formation of epithelial somite and dermomyotome. These results also indicate that PSM cells with different characteristics are rapidly sorted during somite formation.

Subsequent examination of transverse sections confirmed the elimination of Mesp1/Mesp2 double-null cells from dermomyotome (Fig. 5G,H). In the mature somite region, the wild-type dermomyotome-like epithelium was found to form the myotome (my) (Fig. 5I,J). Furthermore, the ventral part of this dermomyotome-like epithelium became mesenchymal and appeared to contribute to the dorsal sclerotome (dsc), implying that this initial dermomyotome-like epithelium actually corresponds to the epithelial somite exclusively composed of wild-type cells (Fig. 5I,J). Fluorescent phalloidin staining revealed that the apical localization of actin filaments is limited to the dorsal compartments, which are occupied by wild-type cells in the Mesp1/Mesp2 double-null chimeric embryo (Fig. 5K,L), indicating the Mesp1/Mesp2 double-null cells cannot undergo epithelialization.

It is known that the bHLH transcription factor paraxis (Tcf15 – Mouse Genome Informatics), is required for the epithelialization of somite and

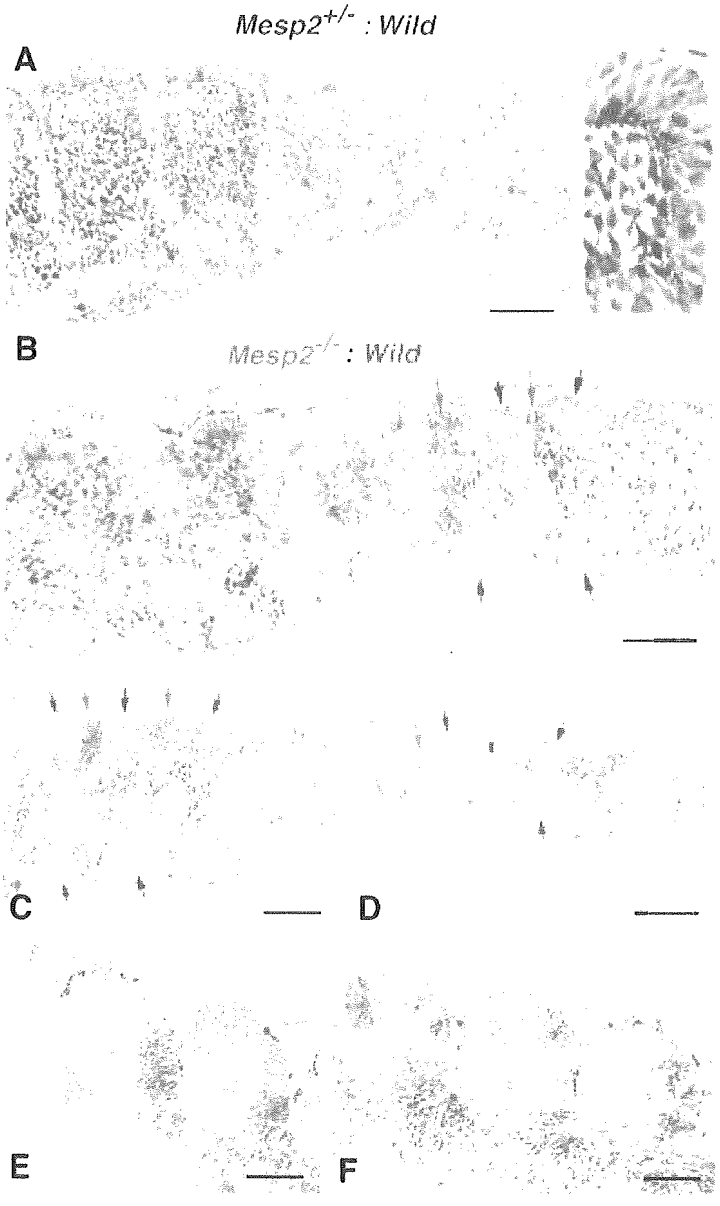

Fig. 3. Mesp2-null cells tend to be excluded from the epithelial region of the somites. (A) The control chimeric embryo undergoes normal somite formation and shows random distribution of labeled cells. The right panel is a high-power view of a somite. (B) In the Mesp2-null chimeric embryo, incompletely segmented somites are formed. Mesp2-null cells tend to be localized at the rostral and central region of these incomplete segments. Red arrows: wild-type cell clusters; blue arrows: Mesp2-null cell clusters. (C,D) Other sections indicating multiple small epithelial cell clusters (arrows). Note that Mesp2-null cells only partially contribute to the epithelial clusters (blue arrows). (E,F) A small number of Mesp2-null cells are distributed in the dermomyotome and are mostly localized at the caudal end. Scale bars: 100 μm.

dermomyotome (Burgess et al., 1995; Burgess et al., 1996). Although *Paraxis* expression is not affected in Mesp2-null embryos (data not shown), it is possible that it is influenced by the loss of both Mesp1 and Mesp2. We therefore examined the expression patterns of *Paraxis* in our Mesp1/Mesp2 double-null chimeras. In wild-type embryos *Paraxis* is initially expressed throughout the entire somite region (in both the prospective dermomyotomal and sclerotomal regions) in the anteriormost PSM and newly forming somites, and then localizes in the dermomyotomes (Burgess et al., 1995). The dorsal dermomyotomal epithelium, composed of wild-type cells, strongly expressed *Paraxis* in the chimeric embryo (Fig. 6A,B). In addition, adjacent sections revealed that *lacZ*-expressing Mesp1/Mesp2 double-null cells expressed *Paraxis* in the medial sclerotomal compartment (Fig. 6A,B, brackets). This suggests that *Paraxis* expression in the future sclerotomal region is independent of Mesp factors. However, at present we cannot exclude the possibility that the maintenance of *Paraxis* expression in the dermomyotome requires the functions of either Mesp1 or Mesp2.

Mesp1/Mesp2 double-null cells are incapable of acquiring rostral properties

To clarify the rostro-caudal properties of somites in our chimeric embryos, we examined the expression pattern of *Uncx4.1*. Control chimeric embryos exhibited a normal stripe pattern of *Uncx4.1* expression throughout the segmented somite region (Fig. 7A). By contrast, Mesp1/Mesp2 double-null chimeric embryos exhibited continuous *Uncx4.1* expression in the ventral sclerotomal region (Fig. 7B). This continuity was observed in the entire sclerotome-like compartment of the newly formed somite region and in the ventral sclerotome in the mature somite region. The caudal localization of *Uncx4.1* expression, however, was normal in the dermomyotome and the dorsal sclerotome, which consisted of wild-type cells (Fig. 5), even in Mesp1/Mesp2 double-null chimeras. This suggests that, like Mesp2-null cells, Mesp1/Mesp2 double-null cells are incapable of acquiring rostral properties. Since the mesoderm of Mesp1/Mesp2 double-null embryos lacks the expression of the major markers of paraxial mesoderm (Kitajima et al., 2000), and Mesp1/Mesp2 double-null cells do not exhibit histological features characteristic of epithelial somites in our current study, it is possible that Mesp1/Mesp2 double-null cells may lack paraxial mesoderm properties. However, the analysis of adjacent sections suggests that *lacZ*-expressing Mesp1/Mesp2 double-null cells themselves express *Uncx4.1*, a somite-specific marker (Fig. 7C,D), and they had also been found to have normal expression of *Paraxis* (Fig. 6A,B).

It is believed that the rostro-caudal pattern within somites and dermomyotomes is generated in the PSM and maintained in somites and dermomyotomes. We observed a normal rostro-caudal pattern in the dermomyotome (Fig. 7), although wild-type cells and Mesp1/Mesp2 double-null cells are mixed in the PSM (Fig. 5), of Mesp1/Mesp2 double-null chimeric embryos. As Mesp products are required for suppression of *Dll1* in the anterior PSM, a normal Dll1 stripe pattern cannot be formed if Mesp1/Mesp2 double-null cells are randomly distributed in

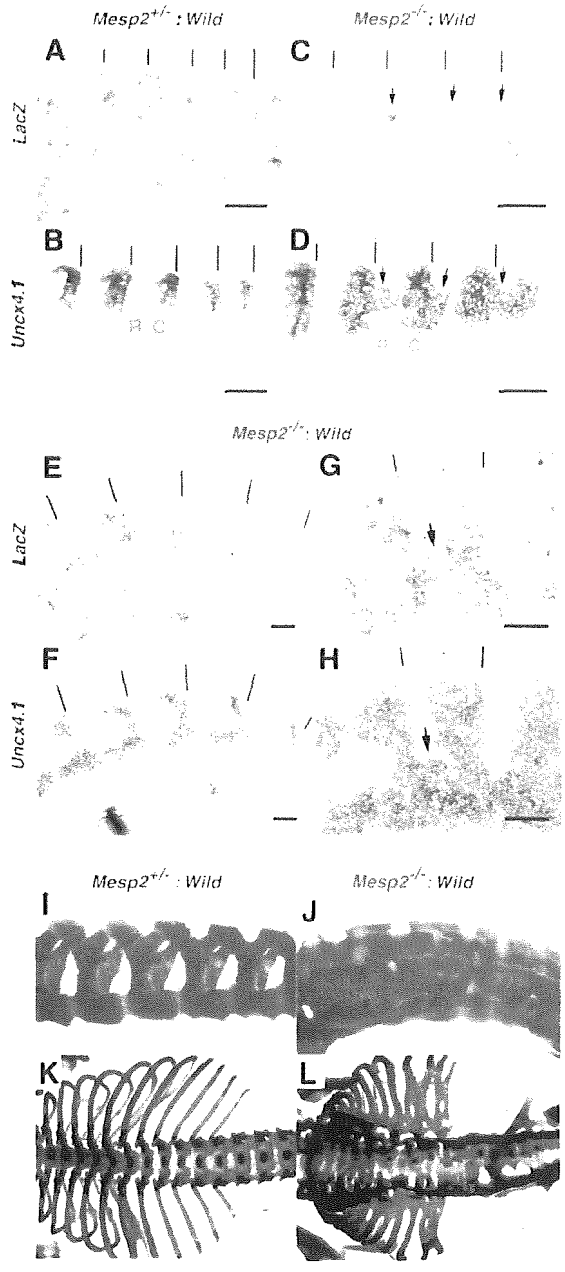

Fig. 4. Mesp2 function is cell autonomously required for rostral properties. (A-D) Expression of *lacZ* and *Uncx4.1* transcripts at the site of initial somite formation in control (A,B) and Mesp2-null (C,D) chimeric embryos. In the control, *lacZ*-expressing cells are randomly distributed and *Uncx4.1* expression is normal. In the Mesp2-null chimera, *lacZ*-expressing Mesp2-null cells at the rostral part of the incomplete segments (arrows in C) ectopically express *Uncx4.1* (arrows in D). Lines indicate somite boundaries. (E,F) In the dermomyotome, Mesp2-null cells are mostly localized at the caudal end, and the *Uncx4.1* expression pattern is normal. (G,H) In the sclerotome, the distribution of Mesp2-null cells results in expansion of *Uncx4.1* expression (arrows). (I) The control chimeric fetus shows normal vertebrae. (J) The Mesp2-null chimeric fetus exhibits partial fusion of the neural arches. (K) The control chimeric fetus shows normal ribs. (L) The Mesp2-null chimeric fetus shows proximal rib fusion. Scale bars: 100 μm. C, caudal compartment; R, rostral compartment.

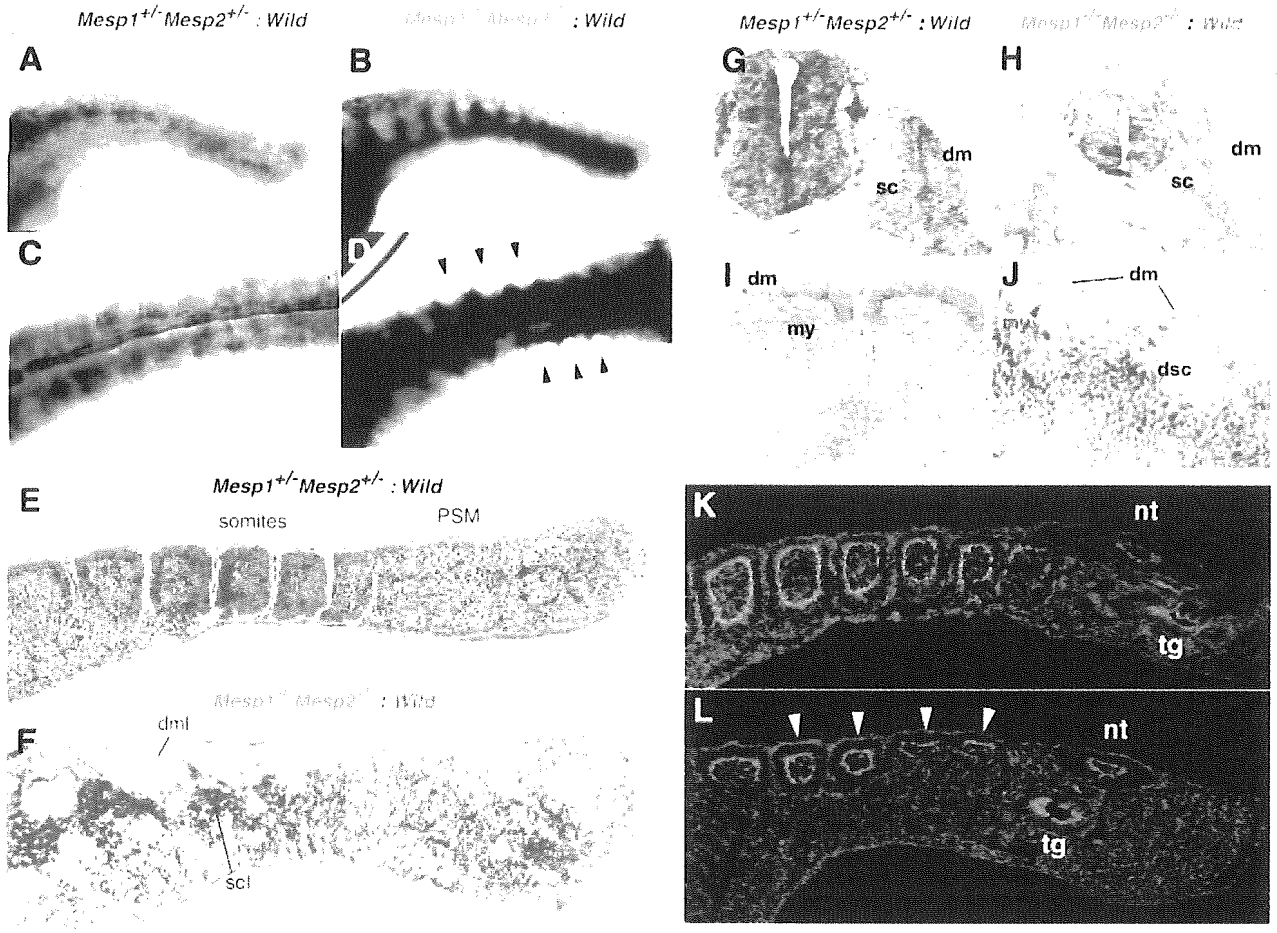

Fig. 5. Mesp1/Mesp2 double-null cells fail to contribute to epithelial somites or to the dermomyotome. (A-D) Tail regions from X-gal-stained whole-mount specimens of control (A,C) and double-null (B,D) chimeric embryos. (A,B) Lateral view. (C,D) Dorsal view. The blue double-heterozygous cells are randomly distributed in the control embryo, whereas the Mesp1/Mesp2 double-null cells are excluded from the lateral region of the somites (arrowheads in D). (E,F) Parasagittal sections of tails from chimeric embryos. (E) The labeled cells are randomly located in the control chimera. (F) The two types of cells are randomly mixed in the PSM, whereas the dermomyotome-like epithelium consisted exclusively of wild-type cells and the sclerotome-like compartment contained mostly Mesp1/Mesp2 double-null cells. Note that normal epithelial somites are not formed in this chimera. (G,H) Transverse sections show elimination of Mesp1/Mesp2 double-null cells from the dermomyotome. (I,J) The dermomyotome-like epithelium in the Mesp1/Mesp2 double-null chimeric embryo gives rise to dermomyotome, myotome (arrowhead in J) and the dorsal part of the sclerotome. Red arches indicate the inner surface of dermomyotome. (K,L) AlexaFluor 488-labeled phalloidin staining shows normal epithelialization of somites in the control chimera (K) and restriction of epithelialization in the dermomyotome-like compartment in the Mesp1/Mesp2 double-null chimera (L). dm, dermomyotome; dml, dermomyotome-like epithelium; dsc, dorsal part of the sclerotome; my, myotome; nt, neural tube; sc, sclerotome; scl, sclerotome-like compartment; tg, tail gut.

the anterior PSM. This is because 50% of cells cannot undergo suppression of Dll1 even in the future rostral half region. Therefore, our finding of a normal rostro-caudal pattern in the dermomyotome of double-null chimeras is surprising and raises the question of whether wild-type cells can be normally patterned in the presence of surrounding Mesp1/Mesp2 double-null cells. To determine how the rostro-caudal pattern in the dermomyotome is formed in the PSM, we examined the expression pattern of *Dll1* (Bettenhausen et al., 1995), the stripe expression profile of which is established in the anteriormost PSM via the function of Mesp2 (Takahashi et al., 2000). The *lacZ*-expressing Mesp1/Mesp2 double-null cells were subsequently found to be consistently localized in the sclerotome-like region, where *Dll1* expression was abnormally expanded (Fig. 6C,D). In the dermomyotome-like region, however, *Dll1* expression in the caudal half was normal. Intriguingly, strong *Dll1* expression in the anteriormost PSM was suppressed in a rostrally adjoining cell population, which is mainly occupied by wild-type cells (Fig. 6C,D, arrows). This implies that wild-type cells and Mesp1/Mesp2 double-null cells rapidly segregate at S-1 to S0, after which the rostro-caudal pattern of *Dll1* expression is formed in the partially segregated wild-type cell population but not in the randomly mixed cell population. In other words, the separation from Mesp1/Mesp2 double-null cells enabled normal rostro-caudal patterning of wild-type cells.

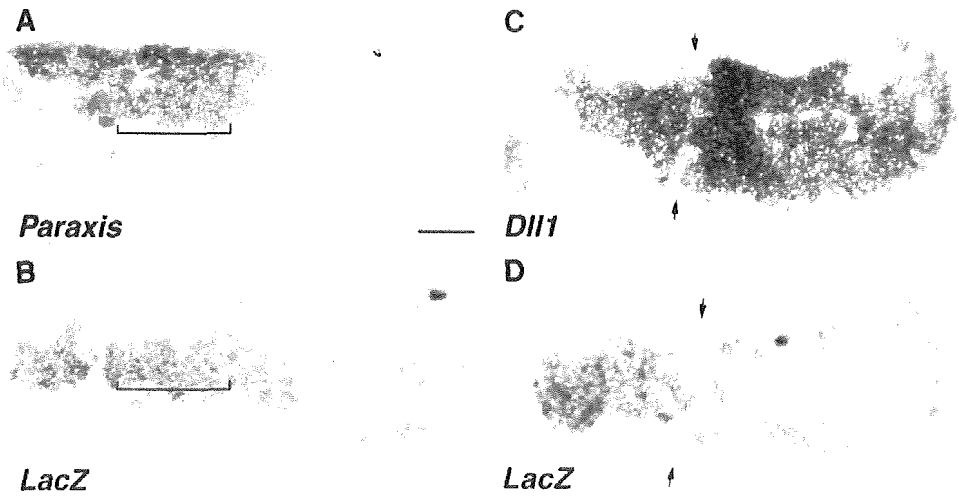

Fig. 6. (A,B) Mesp1/Mesp2 double-null cells express *Paraxis*. Adjacent parasagittal sections of the Mesp1/Mesp2 double-null chimeric embryo were stained for either *Paraxis* (A) or *lacZ* (B). Note that the expression domains of the two genes overlap in the medial sclerotomal region (brackets). (C,D) The rostro-caudal pattern in the dermomyotome is formed in a partially segregating wild-type cell population. Adjacent sections of the Mesp1/Mesp2 double-null chimeric embryos were stained for *Dll1* (C) or *lacZ* (D) mRNA. Red outlines demarcate the dorsal dermomyotome-like compartments. Note that suppression of *Dll1* expression occurs in a region mostly occupied by wild-type cells (arrows). Scale bar: 100 μm.

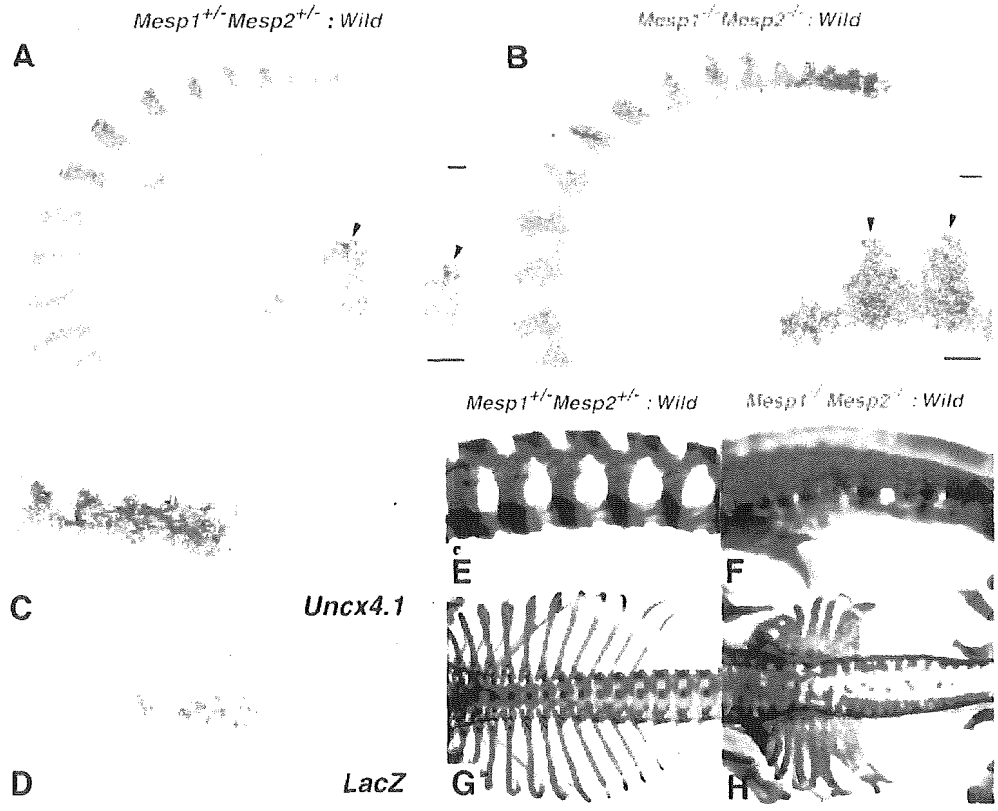

Fig. 7. Rostro-caudal patterning of the sclerotome is disrupted in Mesp1/Mesp2 double-null chimeric embryos. (A) The control chimeric embryos exhibit normal stripe patterns of *Uncx4.1* expression throughout the somite region. (B) The Mesp1/Mesp2 double-null chimeric embryos exhibit continuous *Uncx4.1* expression in the ventral sclerotomal region. Note that caudal localization of *Uncx4.1* expression is normal in the dermomyotome and dorsal sclerotome. The insets show a higher magnification of lumbar somites. (C,D) Adjacent sections showing that *lacZ*-expressing Mesp1/Mesp2 double-null cells express *Uncx4.1*. (E-H) The Mesp1/Mesp2 double-null chimeric fetus exhibits caudalization of the vertebrae and of the proximal ribs. (E) The control chimeric fetus shows normal metameric arrangement of the neural arches. (F) The Mesp1/Mesp2 double-null chimeric fetus shows severe fusion of the pedicles and the laminae of neural arches. (G) The control chimeric fetus has normal arrangement of ribs. (H) The double-null chimeric fetus shows severe fusion of the proximal elements of the ribs. Scale bars: 100 μm.

Mesp2-null fetuses display caudalized vertebrae with extensive fusion of the pedicles of neural arches and proximal elements of the ribs (Saga et al., 1997). The Mesp1/Mesp2 double-null chimeric fetuses also exhibited fusion of the pedicles of neural arches and the proximal ribs (Fig. 7E-H). Furthermore, the vertebrae of severe chimeric fetuses were indistinguishable from those of Mesp2-null fetuses. These observations indicate that Mesp1/Mesp2 double-null cells can differentiate into caudal sclerotome and possibly contribute to chondrogenesis.

Discussion

Mesp1 and Mesp2 not only exhibit similar expression patterns but also share common bHLH domains as transcription factors. Previous studies using gene replacement experiments (Saga, 1998) (Y.S. and S.K., unpublished) indicate that these genes can compensate for each other. However, the early lethality of double knockout mice hampered any further detailed analysis of somitogenesis. An obvious strategy to further elucidate the functions of Mesp1 and Mesp2 was, therefore, the generation of a conditional knockout allele for *Mesp2* in *Mesp1* disrupted cells in which the Cre gene is specifically activated in the paraxial mesoderm, which is now underway. Chimera analysis is also a powerful method as an alternative strategy. Comparisons of chimeras, composed of either Mesp2-null or Mesp1/Mesp2 double-null cells, made it possible to determine the contribution of Mesp1 to somitogenesis. Our results indicate that Mesp1 has redundant functions in the epithelialization of somitic mesoderm and additionally, by chimeric analysis, we were able to demonstrate the cell autonomy of Mesp1 and Mesp2 function during some critical steps of somitogenesis.

The relative contributions of Mesp1 and Mesp2 to somitogenesis

In Mesp1-null mice, epithelial somites with normal rostro-caudal polarity are generated, whereas Mesp2-null mice exhibit defects in both the generation of epithelial somites and the establishment of rostro-caudal polarity. Thus, it seems likely that Mesp2 function is both necessary and sufficient for somitogenesis. However, dermomyotome formation was observed, without normal segmentation, even in Mesp2-null mice. In view of the apparent redundant functions of Mesp1 and Mesp2 in somitogenesis, as demonstrated by our previous gene replacement study, it was possible that the Mesp1/Mesp2 double-null embryo would exhibit a much more severe phenotype in relation to somitogenesis. In our chimera analyses, both Mesp2-null and Mesp1/Mesp2 double-null cells exhibited complete caudalization of somitic mesoderm, indicating that Mesp1 function is not sufficient to rescue Mesp2 deficiency and restore rostro-caudal polarity. Likewise, both Mesp2-null and Mesp1/Mesp2 double-null cells were incapable of forming an initial segment boundary, showing that the contribution of Mesp1 is also minor during this process. By contrast, whereas Mesp1/Mesp2 double-null cells lacked any ability to epithelialize, Mesp2-null cells were occasionally integrated into epithelial somites and dermomyotome, indicating that the contribution of Mesp1 to epithelialization is significant and that Mesp1 can function in the absence of Mesp2 (Fig. 8). We therefore postulate that the epithelialization of dermomyotome, observed in Mesp2-null embryos, is dependent on Mesp1.

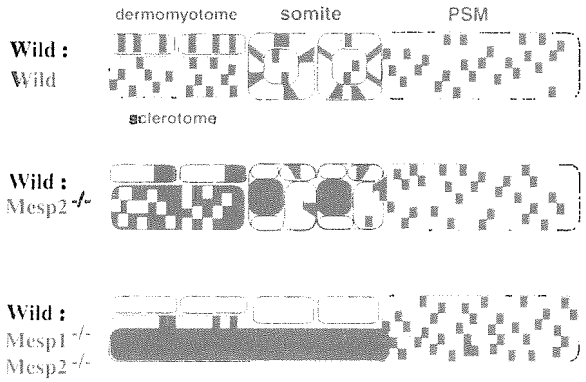

Fig. 8. A schematic summarization of the Mesp1/Mesp2 chimera experiments. Mesp1/Mesp2 double-null cells can contribute to neither epithelial somite nor dermomyotome formation, whereas Mesp2-null cells can partially contribute to both somites and dermomyotome. Red outlines indicate epithelialized tissues (epithelial somites, dermomyotomes and abnormal small clusters).

Mesp factors are cell autonomously required for epithelialization of somitic mesoderm but may also be non-cell autonomously required for morphological boundary formation

Conventional interpretations of the results of chimera analysis are generally based upon the regulative development of the vertebrate embryo and argue cell autonomy of specific gene functions in embryogenesis (Ciruna et al., 1997; Brown et al., 1999; Kitajima et al., 2000; Koizumi et al., 2001). Mesp1/Mesp2 double-null cells failed to form epithelial somites, even in the presence of surrounding wild-type cells. In addition, they were incapable of contributing to dermomyotome, where cell sorting occurs. This strongly suggests that Mesp factors are cell autonomously required for the epithelialization of somitic mesoderm. However, we also found striking non-cell autonomous effects of Mesp mutant cells on wild-type cell behaviors. That is, both types of Mesp mutant cell not only failed to undergo normal somitogenesis, but also inhibited the normal morphogenesis of wild-type cells. This implies that there are non-cell autonomous roles for Mesp factors in the establishment of the future somite boundary, as we will discuss further.

Initial epithelial somite formation is achieved by the mesenchymal-epithelial transition of cells located in the anterior PSM. A future somite boundary is established at a specific position in the PSM, followed by gap formation between the mesenchymal cell populations. Subsequently, cells located anterior to the boundary are epithelialized. This process is known to be mediated by an inductive signal from cells posterior to the boundary (Sato et al., 2002). Therefore, defects in epithelial somite formation can be explained in two principal ways: a lack of cellular ability to epithelialize (cell autonomous) and a lack of an inducing signal, which is produced in the anterior PSM by a mechanism mediated by Notch signaling (thus non-cell autonomous). In the case of chimeras of Mesp1/Mesp2 double-null cells, no local

boundary formed by locally distributed wild-type cells was observed, i.e. even a gap between wild-type cells was never observed in the mixture of Mesp1/Mesp2 double-null cells and wild-type cells. It is likely, therefore, that the wild-type cell population can form a boundary only after separation from Mesp1/Mesp2 double-null cells (Fig. 8). By contrast, some local boundaries between epithelial wild-type cell clusters were occasionally observed in chimeras with Mesp2-null cells. Considering that there is functional redundancy between these transcription factors, it is possible that either Mesp1 or Mesp2 is necessary for the formation of a signaling center or source of the putative inductive signal. Hence, we cannot exclude the possibility that the lack of Mesp function may affect non-cell autonomous generation of the inductive signal in the anterior PSM.

Formation of epithelial somites requires paraxis, which is a transcription factor (Burgess et al., 1996; Nakaya et al., 2004). We observed that Mesp1/Mesp2 double-null cells at the medial sclerotomal region expressed *Paraxis*, indicating that Mesp factors are not absolutely required for *Paraxis* expression. Defects in epithelial somite formation in paraxis-null embryos, with normal *Mesp2* expression (Johnson et al., 2001), and in Mesp2-null embryos, with normal *Paraxis* expression, imply that epithelial somite formation independently requires both gene functions.

Mesp2 is cell autonomously required for the acquisition of rostral properties

The distribution of Mesp2-null cells in the Mesp2-null chimeric embryos may appear somewhat paradoxical, as they are localized at the rostral side in the incomplete somites but at the caudal side in the dermomyotome. Initial localization at the rostral and central region, however, is likely to be due to the relative lack of epithelialization functions. In mammalian and avian embryos, mesenchymal-to-epithelial conversion of the PSM commences from the rostral side of the future somite boundary, i.e. the caudal margin of the presumptive somite (Duband et al., 1987). Epithelialization then proceeds anteriorly in the dorsal and ventral faces and in such a process, Mesp2-null cells, which are less able to participate in epithelialization, may therefore be pushed to the central and rostral sides. Thus, the majority of the Mesp2-null cells localize to the central, prospective sclerotomal region and a small number of them are integrated in the future dermomyotomal region. The incomplete somites then undergo reorganization into dermomyotome and sclerotome, and small numbers of Mesp2-null cells in the dermomyotome may be sorted out to the caudal end. Therefore, the apparently complex distribution pattern of Mesp2-null cells is likely to reflect a combination of defects in epithelialization and rostro-caudal patterning. In the incomplete segments of Mesp2-null chimeric embryos, the Mesp2-null cells fail to acquire rostral properties even when localized at the rostral side. Moreover, in the dermomyotome, where rostro-caudal patterning is rescued, Mesp2-null cells are mostly localized in the caudal region. These observations suggested that the requirement of Mesp2 for the acquisition of rostral properties is cell autonomous. Similarly, it has been reported that presenilin 1 (Psen1) is required for acquisition of caudal half properties (Takahashi et al., 2000; Koizumi et al., 2001) and that Psen1-null cells cannot contribute to the caudal half of somites in chimeric embryos, showing cell autonomous roles for Psen1 (Koizumi et al., 2001).

Mesp mutant cells affect the rostro-caudal patterning of somites due to the lack of cellular interaction with wild-type cells

In a previous study, we have shown that the rostro-caudal patterning of somites is generated by complex cellular interactions involved in positive and negative feedback pathways of Dll1-Notch and Dll3-Notch signaling, and regulation by Mesp2 in the PSM (Takahashi et al., 2003). In chimeras with either Mesp2-null or Mesp1/Mesp2 double-null cells, the mutant cells were distributed evenly and did not show any sorting bias in a rostro-caudal direction in the PSM. Since both Mesp2-null and Mesp1/Mesp2 double-null cells have the ability to form caudal cells, it is likely that if wild-type cells could occupy the rostral part of future somite regions and have the ability to sort in the PSM, a normal rostro-caudal patterning would be generated. We did not observe this, however, and conclude that the presence of mutant cells lacking Mesp factors must have disrupted normal cellular interactions via Notch signaling. Thus these non-cell-autonomous effects of our mutant cells are strongly supportive of our previous contention that rostro-caudal pattering is generated by cellular interactions via Notch signaling.

We thank Mariko Ikumi, Seiko Shinzawa, Eriko Ikeno and Shinobu Watanabe for general technical assistance. This work was supported by Grants-in-Aid for Science Research on Priority Areas (B) and the Organized Research Combination System of the Ministry of Education, Culture, Sports, Science and Technology, Japan.

References

Bettenhausen, B., Hrabe de Angelis, M., Simon, D., Guénet, J.-L. and Gossler, A. (1995). Transient and restricted expression during mouse embryogenesis of Dll1, a murine gene closely related to *Drosophila* Delta. *Development* **121**, 2407-2418.

Borycki, A. G. and Emerson, C. P., Jr (2000). Multiple tissue interactions and signal transduction pathways control somite myogenesis. *Curr. Top. Dev. Biol.* **48**, 165-224.

Brown, D., Wagner, D., Li, X., Richardson, D. A. and Olson, E. N. (1999). Dual role of the basic helix-loop-helix transcription factor scleraxis in mesoderm formation and chondrogenesis during mouse embryogenesis. *Development* **126**, 4317-4329.

Burgess, R., Cserjesi, P., Ligon, K. L. and Olson, E. N. (1995). Paraxis: a basic helix-loop-helix protein expressed in paraxial mesoderm and developing somites. *Dev. Biol.* **168**, 296-306.

Burgess, R., Rawls, A., Brown, D., Bradley, A. and Olson, E. N. (1996). Requirement of the *paraxis* gene for somite formation and musculoskeletal patterning. *Nature* **384**, 570-573.

Ciruna, B. G., Schwartz, L., Harpal, K., Yamaguchi, T. P. and Rossant, J. (1997). Chimeric analysis of *fibroblast growth factor receptor-1 (Fgfr1)* function: a role for FGFR1 in morphogenetic movement through the primitive streak. *Development* **124**, 2829-2841.

Duband, J. L., Dufour, S., Hatta, K., Takeichi, M., Edelman, G. M. and Thiery, J. P. (1987). Adhesion molecules during somitogenesis in the avian embryo. *J. Cell Biol.* **104**, 1361-1374.

Fan, C. M. and Tessier Lavigne, M. (1994). Patterning of mammalian somites by surface ectoderm and notochord: Evidence for sclerotome induction by a hedgehog homolog. *Cell* **79**, 1175-1186.

Gossler, A. and Hrabe de Angelis, M. (1997). Somitogenesis. *Curr. Top. Dev. Biol.* **38**, 225-287.

Johnson, J., Rhee, J., Parsons, S. M., Brown, D., Olson, E. N. and Rawls, A. (2001). The anterior/posterior polarity of somites is disrupted in Paraxis-deficient mice. *Dev. Biol.* **229**, 176-187.

Kitajima, S., Takagi, A., Inoue, T. and Saga, Y. (2000). MesP1 and MesP2

are essential for the development of cardiac mesoderm. *Development* **127**, 3215-3226.

Koizumi, K., Nakajima, M., Yuasa, S., Saga, Y., Sakai, T., Kuriyama, T., Shirasawa, T. and Koseki, H. (2001). The role of presenilin 1 during somite segmentation. *Development* **128**, 1391-1402.

Mansouri, A., Yokota, Y., Wehr, R., Copeland, N. G., Jenkins, N. A. and Gruss, P. (1997). Paired-related murine homeobox gene expressed in the developing sclerotome, kidney, and nervous system. *Dev. Dyn.* **210**, 53-65.

Nakaya, Y., Kuroda, S., Katagiri, Y. T., Kaibuchi, K. and Takahashi, Y. (2004). Mesenchymal-epithelial transition during somitic segmentation is regulated by differential roles of Cdc42 and Rac1. *Dev. Cell* **7**, 425-438.

Neidhardt, L. M., Kispert, A. and Herrmann, B. G. (1997). A mouse gene of the paired-related homeobox class expressed in the caudal somite compartment and in the developing vertebral column, kidney and nervous system. *Dev. Genes Evol.* **207**, 330-339.

Nieto, M. A., Gilardi-Hebenstreit, P., Charnay, P. and Wilkinson, D. G. (1992). A receptor protein tyrosine kinase implicated in the segmental patterning of the hindbrain and mesoderm. *Development* **116**, 1137-1150.

Nomura-Kitabayashi, A., Takahashi, Y., Kitajima, S., Inoue, T., Takeda, H. and Saga, Y. (2002). Hypomorphic *Mesp* allele distinguishes establishment of rostro-caudal polarity and segment border formation in somitogenesis. *Development* **129**, 2473-2481.

Pourquié, O. (2001). Vertebrate somitogenesis. *Annu. Rev. Cell. Dev. Biol.* **17**, 311-350.

Saga, Y. (1998). Genetic rescue of segmentation defect in MesP2-deficient mice by MesP1 gene replacement. *Mech. Dev.* **75**, 53-66.

Saga, Y. and Takeda, H. (2001). The making of the somite: molecular events in vertebrate segmentation. *Nat. Rev. Genet.* **2**, 835-845.

Saga, Y., Hata, N., Kobayashi, S., Magnuson, T., Seldin, M. and Taketo, M. M. (1996). MesP1: A novel basic helix-loop-helix protein expressed in the nascent mesodermal cells during mouse gastrulation. *Development* **122**, 2769-2778.

Saga, Y., Hata, N., Koseki, H. and Taketo, M. M. (1997). *Mesp2*: a novel mouse gene expressed in the presegmented mesoderm and essential for segmentation initiation. *Genes Dev.* **11**, 1827-1839.

Saga, Y., Miyagawa-Tomita, S., Takagi, A., Kitajima S., Miyazaki, J. and Inoue, T (1999). MesP1 is expressed in the heart precursor cells and required for the formation of a single heart tube. *Development* **126**, 3437-3447.

Sato, Y., Yasuda, K. and Takahashi, Y. (2002). Morphological boundary forms by a novel inductive event mediated by Lunatic fringe and Notch during somitic segmentation. *Development* **129**, 3633-3644.

Takahashi, Y., Koizumi, K., Takagi, A., Kitajima, S., Inoue, T., Koseki, H. and Saga, Y. (2000). Mesp2 initiates somite segmentation through the Notch signalling pathway. *Nat. Genet.* **25**, 390-396.

Takahashi, Y., Inoue, T., Gossler, A. and Saga, Y. (2003). Feedback loops comprising Dll1, Dll3 and Mesp2, and differential involvement of Psen1 are essential for rostrocaudal patterning of somites. *Development* **130**, 4259-4268.

Zambrowicz, B. P., Imamoto, A., Fiering, S., Herzenberg, L. A., Kerr, W. G. and Soriano, P. (1997). Disruption of overlapping transcripts in the ROSA beta geo 26 gene trap strain leads to widespread expression of beta-galactosidase in mouse embryos and hematopoietic cells. *Proc. Natl. Acad. Sci. USA* **94**, 3789-3794.